Feature Detection in Vector Fields Using the Helmholtz-Hodge Decomposition

Diploma-Thesis

http://www.karman.au.com/dorothy/cruise-2912.html

Author:	Alexander Wiebel
Supervisor:	Dr. Gerik Scheuermann
	Dipl.-Math. Christoph Garth
Organization:	University of Kaiserslautern (TU)
	Fachbereich Informatik
	AG Visualisierungssysteme
	Postfach 3049
	D-67653 Kaiserslautern
	Deutschland

Acknowledgments

I want to thank Gerik Scheuermann for all the time and work he spend supervising my work on this thesis. A support like his, for example the at least weekly meetings, is not usual.

Next I want to thank Christoph Garth for all the fruitful discussions, help and especially for his tutorials in various mathematical areas. Without him the work with *FAnToM* would not have been so easy.

For many ideas, discussions and explanations concerning visualization and related topics, special thanks go to Xavier Tricoche. Last but not least, I would like to thank the whole visualization group of Kaiserslautern for the pleasant atmosphere.

Contents

List of Figures

Chapter 1

Introduction

Fluids[1] are ubiquitous in industry and nature. Analysis of fluid flow is thus a wide scope for research. Indeed, there are many different fields in science which are concerned with fluid mechanics.

A very large area is mechanical engineering. As the behavior of the flow around a moving body is responsible for the aerodynamic resistance, fluid dynamical experiments are important for car design. Apart from the resistance, flows can have negative effects on parts of car. Vortices reaching parts can induce strong vibrations. Even destruction of components can be the result if vortices hitting the car are not detected and eliminated.

Similar experiments have to be undertaken by engineers employed with aviation. Here it is mainly the lift for plains which is interesting. Most lift is generated by the shape of wings, but vortices can play a big role for the lift too. For aircrafts, for example the ones having the delta wing geometry presented later, the vortices are elementary for the lift. They are not desired to be eliminated, in contrary they are desired to exist permanently and uniformly. Very crucial flow characteristics for the lift are separation and attachment. Separations of flow at wings at wrong times already have led to air crashes.

The design and theory of combustion processes in engines, in particular the intermixture of gas and air, today also employs fluid mechanical experiments for improvements.

Topics concerned about flow too, which have nothing to do with engineering, are ocean sciences and meteorology. It is obvious that everything happening in an ocean is influenced by floating water. The floating is generated by differences in temperature, density or by winds on the water surface. This influence of the winds leads to meteorology, as the behavior of air is its central topic. The flow of the air is generated by the rotation of the earth, temperature and differences in pressure.

The theoretical basis for all above mentioned is provided by the fluid mechanics field as it is discussed in mathematics and physics. Research in all the mentioned topics involves experiments with models. The mechanical engineers work with prototypes. Small models of

[1]gases and liquids

the object of research are used by both, natural scientists and mechanical engineers.

Today branches of computer science are gaining influence in all fluid dynamical research areas. The most important branch is computational fluid dynamics (CFD), where the laws of fluid mechanics are used to simulate flow. As CFD involves sophisticated mathematical methods and needs computers for the calculation intensive simulations, it can be seen simultaneously as part of mathematics and computer science. CFD simulations can be employed for all research efforts concerned with flow. The use of CFD in science increases because the simulations are much cheaper than prototypes and experiments with models, they can be modified very much easier and the data produced can be viewed in many different ways.

With the data produced by CFD simulations, the *visualization in scientific computing* comes into play. The data produced by the computations has to be interpreted. A very popular and often cited statement to this comes from Richard Hamming:

> "The purpose of [scientific] computing is insight, not numbers."

McCormick et al. [MDB87] transfer this to visualization:

> The goal of visualization is to leverage existing scientific methods by providing new scientific insight through visual methods.

Visualization in scientific computing or just visualization was first claimed to be an autonomous field of science and research by McCormick et al. [MDB87] in 1987. They define the topic of visualization, justify the demand for efforts in the new field and describe the necessary investments to provide adequate infrastructure for the researchers.

The purpose of visualization is to provide easier insight in data for engineers and scientists. McCormick et al. formulate this as follows:

> Visualization is a method of computing. It transforms the symbolic into the geometric, enabling researchers to *observe* their simulations and computations. [...] It enriches the process of scientific discovery and fosters profound and unexpected insights. [...]

The topic of the present thesis is located in the field of visualization. More precisely the subject of this thesis is feature based visualization[2]. A new method for vortex core extraction and a new approach on detecting attachment and separation lines will be presented. The importance of detecting these features is clear when considering the explanations for car and aircraft design from above.

The developed algorithms were implemented in the visualization program *FAnToM* (**F**ield **An**alysis using **To**pological **M**ethods) [BSTW02]. They use the graphic engine, mathematical infrastructure, data management and the GUI of the program. *FAnToM* is developed in the research group of Dr. Gerik Scheuermann at the University of Kaiserslautern.

[2] The term feature based visualization will be explained in a later chapter.

Both mentioned approaches use a discrete Helmholtz-Hodge decomposition as first step and a ridge and valley lines detection for the final extraction. As the decomposition is limited to tetrahedral domains, both new methods are as well. With the infrastructure of *FAnToM* non-tetrahedral grids can be easily converted into tetrahedral grids. Hence, the mentioned limitation is not a real one, it just implies more preparatory work.

The thesis is structured as follows: Chapter two provides an introductory overview of the used and needed mathematics. Derivatives in multiple dimensions, the gradient, divergence and curl, the various types of fields and some physical interpretations of the mentioned quantities are described. The Helmholtz-Hodge decomposition for the smooth case is introduced.

The focus of chapter three lies on flow features. It explains the ideas of critical points, sinks, sources, vortices and other feature types. The reasons for the development of feature based visualization are given and two vortex detection methods are described. Chapter four details the discrete Helmholtz-Hodge decomposition and a ridges and and valleys extraction algorithm. In chapter five the combination of the decomposition and the extraction, and the algorithms and approaches developed with this combination are described. A theoretical foundation for vortex core detection approach is presented and some results and drawbacks are mentioned.

Chapter six summarizes the results, examples, experiments and drawbacks. Some results and drawbacks are detailed and the presented approaches are compared with common methods. An important drawback of the two dimensional discrete Helmholtz-Hodge decomposition itself is shown. The seventh chapter gives the conclusion and points out opportunities and needs of future work. The appendices contain images from experiments, a formulary and a snapshot of the *FAnToM*-GUI.

Dr. Gerik Scheuermann and Dipl.-Math. Christoph Garth supervised the work on this thesis.

Chapter 2

Vector Analysis

In this chapter we will give a brief introduction into vector analysis. For the following chapters it will be necessary to keep the main ideas of this introduction in mind. Mathematical techniques needed for the derivation of the theoretical foundation for our feature extraction method will be given.

The subject of vector analysis is the differential and integral calculus of vector functions. Thus, one needs the basics of vector algebra, and differentiation and integration in one dimension as basis to follow the introduction. Some assumptions, like a function to be continuous or that some derivatives have to exist, are omitted in the theorems cited in the following.

2.1 Vector functions, vector fields and scalar fields

As mentioned above, vector functions are central for vector analysis. A function f is called a vector function if it maps its argument onto a vector, i.e. $f : D \to \mathbb{R}^m$, $f(d) = \mathbf{v}$ with $d \in D \subset \mathbb{R}^n$ and $\mathbf{v} \in \mathbb{R}^m$.

Vector fields may be accounted as a special case of vector functions. They map vectors to positions of a given volume or area. Technically this is: For a position $\mathbf{r}$ of an area $\mathcal{A}$ or volume $\mathcal{V}$ a vector $\mathbf{v} \in \mathbb{R}^n$ is assigned by $\mathbf{V} : B \to \mathbb{R}^m$, $\mathbf{V}(\mathbf{r}) = \mathbf{v}$ where B represents either $\mathcal{A}$ or $\mathcal{V}$. $\mathbf{V}$ is called vector field. Our focus lies on vector fields where the vectors have two or three dimensions, i.e. $\mathbf{v} \in \mathbb{R}^m, m \in \{2, 3\}$.

Although we primarily deal with vectors, we have to take into account another type of fields. Scalar fields will play a not to small role in this chapter. Scalar fields $U : B \to \mathbb{R}$, $U(\mathbf{r}) = t$ assign scalars $t \in \mathbb{R}$ to the positions $\mathbf{r} \in B$.

2.2 Derivatives and differential operators

Many important properties of vector and scalar fields can be expressed with derivatives of the functions which map scalars or vectors to positions. The first intuitive way defining derivatives for functions of multiple arguments are the partial derivatives.

2.2.1 Partial derivatives, Jacobian and gradient

Let $f : \mathbb{R}^n \to \mathbb{R}^m,\ n, m \in \mathbb{R}$ be a multidimensional vector function. Then its partial derivatives at $\mathbf{x} \in \mathbb{R}^n$ in the directions $x_j,\ 0 < j \leq n$ are defined as

$$\frac{\partial f_i}{\partial x_j}(\mathbf{x}) := \lim_{h \to 0} \frac{f(\mathbf{x} + h\mathbf{e}_j) - f(\mathbf{x})}{h}$$

with $0 < i \leq m$.

The partial derivatives of f form a matrix $\mathcal{J}$, called the Jacobian matrix:

$$\mathcal{J} f(\mathbf{x}) = \left(\frac{\partial f_i}{\partial x_j} \right)_{ij}.$$

For scalar functions, i.e. $m = 1$, the Jacobian reduces to a vector called the gradient:

$$\text{grad } f = \mathcal{J} f = \left(\frac{\partial f}{\partial x_1}, \ldots, \frac{\partial f}{\partial x_n} \right).$$

The vector grad $f(\mathbf{x})$ emanates from $\mathbf{x}$ and points in the direction of the steepest increase of the scalar values.

The Jacobian is sometimes called vector gradient because its rows are the gradients of the scalar component functions of f. This is expressed in formulas as

$$\nabla f = \text{grad } f = \mathcal{J} f = \begin{pmatrix} \text{grad } f_1 \\ \vdots \\ \text{grad } f_m \end{pmatrix}.$$

Directional derivatives

The partial derivatives for $x_1, \ldots, x_n$ are also called directional derivatives in the directions of $\mathbf{e}_1 \ldots \mathbf{e}_n$. They measure the rate of change when going in the direction of the vector $\mathbf{e}_i$ they belong to.

Directional derivatives for directions $\mathbf{d} \in \mathbb{R}^n$ different from $\mathbf{e}_1, \ldots, \mathbf{e}_n$ are defined by

$$\frac{\partial f}{\partial \mathbf{d}} = \text{grad } f \cdot \hat{\mathbf{d}},$$

with "·" being the scalar product and $\hat{\mathbf{d}}$ a unit vector in the direction of $\mathbf{d}$.

2.2.2 Differential operators

The nabla operator

Having established the partial derivatives, we define

$$\nabla = \left(\frac{\partial}{\partial x_1}, \cdots, \frac{\partial}{\partial x_n}\right)^T.$$

The symbol denotes an operator. It appears, for example, in a notation for the gradient: grad $f = \nabla f$. For a 3D scalar field $U : \mathbb{R}^3 \to \mathbb{R}$, ∇U represents the field of the gradients

$$\nabla U(x_1, x_2, x_3) = \begin{pmatrix} \frac{\partial U(x_1,x_2,x_3)}{\partial x_1} \\ \frac{\partial U(x_1,x_2,x_3)}{\partial x_2} \\ \frac{\partial U(x_1,x_2,x_3)}{\partial x_3} \end{pmatrix} = \text{grad } U(x_1, x_2, x_3)$$

at all positions $(x_1, x_2, x_3) \in \mathbb{R}^3$.

Divergence

The Jacobian $\mathcal{J}$ contains the information of most differential operators. Its diagonal elements, for example, contain the divergence.

As $\mathcal{J}$ is a quadratic matrix for our fields, its trace $\text{Tr}(\mathcal{J})$ may be computed. For vector fields with $m > 1$ we define the divergence of f:

$$\text{div } f = \text{Tr}(\mathcal{J} f) = \sum_{i=1}^{n} \mathcal{J}_{ii} = \frac{\partial f_1}{\partial x_1} + \ldots + \frac{\partial f_n}{\partial x_n}. \tag{2.1}$$

Using the nabla operator, this can be written as

$$\text{div } f = \nabla \cdot f$$

where "·" represents the scalar product.

For a vector field $\mathbf{V}$ the Gauss Theorem, also known as divergence theorem, relates the vectors on the boundary $\partial\mathcal{V} = \mathcal{A}$ of a region $\mathcal{V}$ to the divergence in the region:

$$\int_{\mathcal{V}} \text{div } \mathbf{V} d\mathcal{V} = \int_{\mathcal{A}} \mathbf{V} \cdot \mathbf{n} \, d\mathcal{A}$$

with $\mathbf{n}$ beeing the outward normal of the boundary. The theorem holds for $\mathcal{V} \subset \mathbb{R}^i, i \in \{2, 3\}$. In words, it states that the influx and outflux integrated over the boundary is equal to the divergence in the region. This leads to a physical interpretation of the divergence. Shrinking $\mathcal{V}$ to a point in the theorem yields that the divergence at a point may be treated as the material generated at that point.

Curl

Another differential operator, the curl, may be defined using the Jacobian $\mathcal{J}$ too. Note that the definition is only for two and three dimensions.

The Jacobian can be decomposed in a symmetric part $\mathcal{J}^S f$ and an antisymmetric part $\mathcal{J}^A f$ as follows:

$$\begin{aligned} \mathcal{J}^S &= \frac{1}{2}(\mathcal{J}f + (\mathcal{J}f)^T), \\ \mathcal{J}^A &= \frac{1}{2}(\mathcal{J}f - (\mathcal{J}f)^T). \end{aligned}$$

The antisymmetric part contains the information for the curl. It has the following component representation:

$$\mathcal{J}^A f = \left(\frac{\partial f_i}{\partial x_j} - \frac{\partial f_j}{\partial x_i} \right)_{ij}.$$

The curl is defined as

$$\begin{aligned} \text{curl } f &= \left((\mathcal{J}^A f)_{32}, (\mathcal{J}^A f)_{13}, (\mathcal{J}^A f)_{21}\right) \\ &= \left(\frac{\partial f_3}{\partial x_2} - \frac{\partial f_2}{\partial x_3}, \frac{\partial f_1}{\partial x_3} - \frac{\partial f_3}{\partial x_1}, \frac{\partial f_2}{\partial x_1} - \frac{\partial f_1}{\partial x_2} \right), \end{aligned} \tag{2.2}$$

which, like in the definition of the divergence, can be written with the nabla operator:

$$\text{curl } f = \nabla \times f.$$

The rotation of vector field $\mathbf{V}$ on a surface $\mathcal{A}$ is related to its boundary $\partial\mathcal{A} = \mathcal{L}$ by Stokes' theorem. It says that the curl on $\mathcal{A}$ equals the integrated field over $\mathcal{L}$. This is written as

$$\int\limits_{\mathcal{A}} \mathbf{n} \cdot \text{curl } \mathbf{V} d\mathcal{A} = \oint_{\mathcal{L}} \mathbf{V} \cdot d\mathbf{r}.$$

The applicability of this theorem is limited to two dimensional vector fields.

In the book of Borisenko [BT79] we can find another useful theorem concerning the curl. It is derived from the divergence theorem. Suppose $\mathbf{V} = \mathbf{V}' \times \mathbf{c}$ with $\mathbf{c}$, an arbitrary but fixed vector, substituted into the divergence theorem. Using div $(\mathbf{V}' \times \mathbf{c}) = \mathbf{c} \cdot \text{curl } \mathbf{V}'$, one gets

$$\int\limits_{\mathcal{V}} \text{curl } \mathbf{V}' \, d\mathcal{V} = \int\limits_{\mathcal{A}} \mathbf{n} \times \mathbf{V}' \, d\mathcal{A}$$

Both theorems yield physical interpretations of the curl. Stokes' theorem says that the flow around a region determines the curl and thus the rotation of the fluid in the region. The second theorem yields an interpretation of the curl for a single point: Shrinking the volume $\mathcal{V}$ to a point, the curl vector indicates the axis and magnitude of the rotation of that point.

Laplacian

For curl, div and grad we apply ∇ once. Applying it a second time, we get a set of expressions of which one, namely $\nabla \cdot \nabla$, is also very common in vector analysis. $\nabla \cdot \nabla$ is called the Laplacian operator, written as Δ. The Laplacian of a scalar field is defined as

$$\Delta U = \nabla^2 U = \nabla \cdot \nabla U = \text{div grad } U,$$

$$\Delta U = \frac{\partial^2 V_1}{\partial x_1^2} + \frac{\partial^2 V_2}{\partial x_2^2} + \frac{\partial^2 V_3}{\partial x_3^2},$$

and thus is the divergence of the gradient.

When applied to a vector field, the Laplacian operates component-wise. The Laplacian of a vector field is a vector field. An occurrence of a vector Laplacian can be found in equation B.7. Due to the Laplacian's notation as $\nabla \cdot \nabla$, it can easily be mixed up with the Hessian $\nabla(\nabla U)$, which is the matrix of the second partial derivatives. Laplacian and Hessian are completely different, i.e $\nabla \cdot \nabla \neq \nabla(\nabla U)$. They only share a very similar notation.

Properties of differential operators

Some important properties of differential operators can be found in the appendix B.1. Other properties may be used in the following chapters. They can be found in the literature [BSMM00, BT79]. The properties there are by far to many to repeat them in this thesis.

2.3 Important types of vector fields

In connection with the differential operators vector fields are divided into groups with special characteristics. Of special interest for us will be potential fields, solenoidal fields and Laplacian fields. They are described in this section.

2.3.1 Potential or irrotational fields

A vector field $\mathbf{V}$ is said to be a potential field if there exists a scalar field φ with

$$\mathbf{V} = \text{grad } \varphi = \nabla\varphi.$$

φ is then called the scalar potential of the vector field $\mathbf{V}$.

To understand why the potential fields take an important place in vector analysis, one has to introduce a term describing the topology of the field's domain. This needed term is: simply connected region. A region B is said to be connected if every two points lying in it can be connected with a curve lying completely in it. It is called simply connected if it is connected and every closed curve lying in it can be shrunk continuously to a point without quitting the region.

With this, we have all terminology ready for the following statement which clarifies the importance of potential fields: A vector field $\mathbf{V}$ living on a simply connected region is irrotational, i.e. curl $\mathbf{V} = 0$, if and only if it is a potential field.

It is worth mentioning that the potential defining the potential field is not unique. As

$$\text{grad } (U + c) = \text{grad } U + \text{grad } c = \text{grad } U + 0 = \text{grad } U,$$

the potential is only defined up to a constant.

2.3.2 Solenoidal fields

The above fields can be derived from scalar potentials. Demanding

$$\mathbf{V} = \text{curl } \mathbf{\Phi} = \nabla \mathbf{\Phi}$$

leads to another group of fields, the so called solenoidal fields. Solenoidal fields stem from potentials too, but this time from vector potentials (here $\mathbf{\Phi}$). These fields can describe incompressible fluid flow and are therefore as important as potential fields. A vector field $\mathbf{V}$ is solenoidal, i.e $\mathbf{V} = \nabla \times \mathbf{\Phi}$ with $\mathbf{\Phi} : \mathbb{R}^n \to \mathbb{R}^m$, if and only if the divergence of $\mathbf{V}$ vanishes.

Again, the potential, here the vector potential, is not unique. It is determined only up to a gradient field because with equation B.5

$$\text{curl } (\mathbf{V} + \nabla U) = \text{curl } \mathbf{V} + \text{curl } \nabla U = \text{curl } \mathbf{V} + 0 = \text{curl } \mathbf{V}$$

holds.

2.3.3 Laplacian fields

A vector field $\mathbf{V}$ which is both, solenoidal and potential, is said to be a Laplacian field. In a simply connected region a Laplacian field is the gradient of a scalar potential which satisfies Laplace differential equation $\Delta\varphi = 0$. Since a Laplacian field is solenoidal and potential, it satisfies curl $\mathbf{V} = 0$ and div $\mathbf{V} = 0$.

Solenoidal fields, as mentioned above, stem from vector potentials. Thus for Laplacian fields there, additionally, has to exist a vector potential $\mathbf{\Phi}$ such that $\nabla \times \mathbf{\Phi} = \mathbf{V}$ holds.

Harmonic functions

Scalar functions like φ whose Laplacian vanish, are called harmonic functions. An important property of these functions is that they are completely determined by their boundary values. This means that there exists only one function that satisfies Laplace's equation for fixed boundary values. Especially the following holds:

$$\Delta\varphi = 0 \ \wedge \ \varphi|_{\partial B} = 0 \quad \Rightarrow \quad \varphi = 0 \text{ everywhere in } B.$$

Other properties can be found in appendix B.2 or can be looked up in the literature [BSMM00, BT79].

2.4 Green's formulas

Green's formulas are important for the derivation of the theoretical foundation mentioned at the beginning of this chapter. Hence, we dedicate some attention to them here.

Assume that for the vector field $\mathbf{V}$ in the divergence theorem $\mathbf{V} = \varphi\nabla\psi$ holds. Then, with div $\mathbf{V} = \varphi\Delta\psi + \nabla\varphi \cdot \nabla\psi$ and $\mathbf{V} \cdot \mathbf{n} = \varphi\frac{\partial\psi}{\partial n}$, we get Green's first formula:

$$\int\limits_{\mathcal{V}} (\varphi\Delta\psi + \nabla\varphi \cdot \nabla\psi) d\mathcal{V} = \int\limits_{\mathcal{A}} \varphi \frac{\partial\psi}{\partial n} d\mathcal{A}.$$

If we choose $\mathbf{V} = \varphi\nabla\psi - \psi\nabla\varphi$ we analogously obtain

$$\int\limits_{\mathcal{V}} (\varphi\Delta\psi - \psi\Delta\varphi) d\mathcal{V} = \int\limits_{\mathcal{A}} \left(\varphi\frac{\partial\psi}{\partial n} - \psi\frac{\partial\varphi}{\partial n}\right) d\mathcal{A},$$

which is Green's second formula.

2.5 Helmholtz-Hodge decomposition

In later chapters the terms source, sink and vortex will be explained. They denote features in flow fields. Thinking of curl and divergence as quantities which have to do with sources, sinks and vortices, and knowing that sources, sinks and vortices are important features of flow, leads to the idea of separating them from the rest of the flow. Having a field with only the vortices and another which only contains the sources and sinks could provide deeper insight into the structure of a flow.

In the mathematical theory of fluid dynamics [CM98, AMR88] there exists a method which yields exactly the two fields mentioned above. It is called the Helmholtz-Hodge decomposition.

Due to Tong [TLHD03], the decomposition is formulated in the three dimensional euclidian space as follows: For a vector field $\mathbf{v}$, there exist two potentials $D, \mathbf{R}$ and a vector field $\mathbf{h}$ such that

$$\mathbf{v} = \nabla D + \nabla \times \mathbf{R} + \mathbf{h} \tag{2.3}$$

and

$$\mathbf{v} = \mathbf{d} + \mathbf{r} + \mathbf{h} \tag{2.4}$$

hold. D is a scalar potential with $\nabla D = \mathbf{d}$ and $\mathbf{R}$ is a vector potential with $\nabla \times \mathbf{R} = \mathbf{r}$. To guarantee uniqueness of the decomposition, boundary conditions have to be introduced: grad D is demanded to be normal to the boundary while curl $\mathbf{R}$ has to be tangential to it. Inspecting the fields $\mathbf{d}$ and $\mathbf{r}$, one finds that curl $\mathbf{d} = 0$ and div $\mathbf{r} = \mathbf{0}$. This can be easily seen using the identities B.5 and B.6 from the appendix.

$$\begin{aligned} \text{curl}\ \mathbf{d} &= \nabla \times \mathbf{d} = \nabla \times \nabla D = 0 \\ \text{div}\ \mathbf{r} &= \nabla \cdot \mathbf{r} = \nabla \cdot (\nabla \times \mathbf{R}) = \mathbf{0} \end{aligned}$$

The curl and the divergence of the remaining field **h** both vanish. Due to these properties, **r** is called the rotation component or the divergence-free part of **v**, and **d** is called the curl-free part or divergence component. The remainder **h** is the so-called "harmonic" component. For consistency in terminology, we call **R** the rotation potential and D the divergence potential.

Since

$$\begin{array}{rcccccc} \text{curl } \mathbf{v} & = & \text{curl grad } D & + & \text{curl curl } \mathbf{R} & + & \text{curl } \mathbf{h} \\ & = & 0 & + & \text{curl } \mathbf{r} & + & 0 \end{array},$$

the curl of the rotation component equals the curl of the original field. Analogously, the divergence component has the same divergence as the original field because

$$\begin{array}{rcccccc} \text{div } \mathbf{v} & = & \text{div grad } D & + & \text{div curl } \mathbf{R} & + & \text{div } \mathbf{h} \\ & = & \text{div } \mathbf{d} & + & 0 & + & 0 \end{array}$$

holds.

The decomposition for 2D vector fields requires a different notation. Let J be an operator on vector fields which rotates every vector in the field on which it is applied about 90 degrees in counter-clockwise order. Then

$$\text{curl } J\mathbf{V} = \text{div } \mathbf{V} \tag{2.5}$$

holds. As in two dimensions

$$\text{div } \mathbf{V} = \frac{\partial V_1}{\partial x_1} + \frac{\partial V_2}{\partial x_2}$$

and

$$\text{curl } \mathbf{V} = \frac{\partial V_2}{\partial x_1} - \frac{\partial V_1}{\partial x_2},$$

it follows

$$\begin{aligned} \text{curl } J\mathbf{V} &= \text{curl } J \begin{pmatrix} V_1 \\ V_2 \end{pmatrix} \\ &= \text{curl} \begin{pmatrix} -V_2 \\ V_1 \end{pmatrix} \\ &= \frac{\partial V_1}{\partial x_1} - \left(-\frac{\partial V_2}{\partial x_2} \right) \\ &= \frac{\partial V_1}{\partial x_1} + \frac{\partial V_2}{\partial x_2} \\ &= \text{div } \mathbf{V} \end{aligned}$$

and thus equation 2.5. This yields that a two dimensional divergence free field can be obtained by computing the gradient of a potential and applying J.

Then the Helmholtz-Hodge decomposition in two dimensions is

$$\begin{aligned}\mathbf{v} &= \nabla D + J\nabla R + \mathbf{h} \\ &= \mathbf{d} + \mathbf{r} + \mathbf{h},\end{aligned}$$

where R now is a scalar potential. Again, the curl of $\mathbf{d}$, the divergence of $\mathbf{r}$ and divergence and curl of $\mathbf{h}$ vanish.

Recalling the terminology introduced in the beginning of this chapter, we recognize that the decomposition produces a solenoidal field, a potential field and a Laplacian field. Notice, that the vector potential $\mathbf{R}$ is not solenoidal in general.

2.6 Formulas for the rotation potential

In a later chapter we will discuss a vortex core extraction method. An important property of the rotation potential is needed for the extraction. The goal of this section is to present an equation formulating this property.

By setting the components of the vector field $\mathbf{V}$ in the divergence theorem to

$$V_k = T_{ik}c_i, \tag{2.6}$$

where T_{ik} is a tensor field and $\mathbf{c}$ is an arbitrary vector Borisenko and Tarapov [BT79] infer

$$\int\limits_{\mathcal{V}} \frac{\partial T_{ik}}{\partial x_k} d\mathcal{V} = \int\limits_{\mathcal{A}} T_{ik} n_k d\mathcal{A}. \tag{2.7}$$

Setting

$$T_{ik} = A_i \frac{\partial}{\partial x_k}(\frac{1}{r}) - \frac{1}{r}\frac{\partial A_i}{\partial x_k}$$

in 2.7 they find

$$\mathbf{A}(M_0) = \frac{1}{4\pi}\int\limits_{\mathcal{V}} \frac{1}{r}\Delta\mathbf{A} d\mathcal{V} - \frac{1}{4\pi}\int\limits_{\mathcal{A}} \left[\mathbf{A}\frac{\partial}{\partial n}\left(\frac{1}{r}\right) - \frac{1}{r}(\mathbf{n}\cdot\nabla)\mathbf{A}\right] d\mathcal{A}, \tag{2.8}$$

where $\mathbf{A}$ is a vector field with components A_1, A_2, A_3.

Substituting r by $\frac{1}{|x-x'|}$, replacing $\mathbf{A}$ with the rotation potential $\mathbf{R}$ and considering B as the volume and its boundary ∂B as the surface, we get

$$\begin{aligned}\mathbf{R}(x) = &-\frac{1}{4\pi}\int\limits_{B} \frac{1}{|x-x'|}\Delta\mathbf{R}(x')dx' \\ &-\frac{1}{4\pi}\int\limits_{\partial B} \mathbf{R}(x')\frac{\partial}{\partial n(x')}\left(\frac{1}{|x-x'|}\right)dx' \\ &+\frac{1}{4\pi}\int\limits_{\partial B} \frac{1}{|x-x'|}\frac{\partial \mathbf{R}(x')}{\partial n(x')}dx'.\end{aligned}$$

To eliminate the vector Laplacian and thus for better understanding, identity B.7 is applied:

$$\begin{aligned}
\mathbf{R}(x) &= -\frac{1}{4\pi}\int\limits_{B}\frac{1}{|x-x'|}\text{grad div }\mathbf{R}(x')dx' \\
&\quad +\frac{1}{4\pi}\int\limits_{B}\frac{1}{|x-x'|}\text{curl curl }\mathbf{R}(x')dx' \\
&\quad -\frac{1}{4\pi}\int\limits_{\partial B}\mathbf{R}(x')\frac{\partial}{\partial n(x')}\left(\frac{1}{|x-x'|}\right)dx' \\
&\quad +\frac{1}{4\pi}\int\limits_{\partial B}\frac{1}{|x-x'|}\frac{\partial \mathbf{R}(x')}{\partial n(x')}dx'. \qquad (2.9)
\end{aligned}$$

An analogous formula holds for scalar fields, it can be derived using Green's formulas (see 2.4). To follow the derivation of Borisenko and Tarapov for equation 2.8, parts of the derivation for the scalar formula are needed . The presented equations are only fragments of the derivation. They are only noted to give a hint to the origins of equation 2.8. The complete derivation can be found in the book of Borisenko and Tarapov [BT79].

Chapter 3

Flow Features

In the introduction it was mentioned how the field of visualization came to life and how it was introduced to the scientific research. Visualization today is used in various fields of research and is thus a manifold subject. It can be divided into sub-topics. A very important part is flow visualization. It mainly deals with data which CFD[1]-calculations provide. With the advancing development of computers used for CFD, the data provided by the computations increases at least as much as the power of the computers. Better data structures and larger memory amplify this effect.

The vast amounts of data are the origin of a visualization problem already mentioned by Helman and Hesselink [HH89]. If one visualizes the data using standard techniques like Hedgehogs (a small arrow for every vector in a given vector field) or streamlines (also known as integral curves), a person viewing the produced graphics can not get much information out of it. A hedgehog with millions of arrows, or streamlines in 3D only look like chaos.

There are two main possibilities to avoid this problem. The first, proposed by Helman and Hesselink [HH89], is vector field topology. This approach divides the field into regions of streamlines with similar behavior, by streamlines going from a singular point to another or to the boundary. These lines are called separatrices. Separatrices and the critical points (explained later in this chapter) are displayed to visualize the topology of the field.

Computing the locations of specific features of the flow and showing merely these features by lines, points or other appropriate graphical objects, is the second possibility. It is called feature-based visualization. Instead of millions of small arrows or thousands of knotted streamlines, one only visualizes the areas or points which are characteristic for the flow.

Feature-based approaches can be used in various fields of visualization, but are described here especially for flow visualization because most of the test datasets used for this thesis originate from CFD computations.

[1]CFD: computational fluid dynamics

3.1 Types of features

Before we introduce a classification of features, it is worth mentioning that there does not exist a general definition of what a feature is. The meaning of the word feature varies from one field of interest to the other and, even in a single field, people do not agree in what a feature is. Due to Roth [Rot00], most definitions have in common that a feature at least has to be a pattern or structure of interest in the data. For visualization tasks, it is necessary that a certain feature, which is intended to be visualized, has a mathematical, precise definition. Only with such a definition can a feature be detected automatically. One main task of feature-based visualization is to find the *position* at which a feature is located in the dataset.

3.1.1 Classification

Features may be classified by the kind of description of their position.

Points

Positions of some features, like sinks, sources and 2D vortex centers, can be described by just giving a point. Those features are called critical points (this term will be specified later) and as they are points they are only present at a position.

Lines

3D vortex cores or ridge lines are features which occupy a set of points forming a line. Thus, such features have to be visualized as lines in the data.

Surfaces

Features covering a set of points representing a surface are, for example, shock waves. Iso-surfaces too, could be treated as features whose position is described by surfaces.

Volume

Some features cover more than a point, line or surface, they cover whole regions in 3D. Examples for features visualized as volumes are vortex regions.

3.1.2 Features in fluid flow

Critical points and vortices are among the most important features in flow fields. They will be described in detail in the following.

Critical points

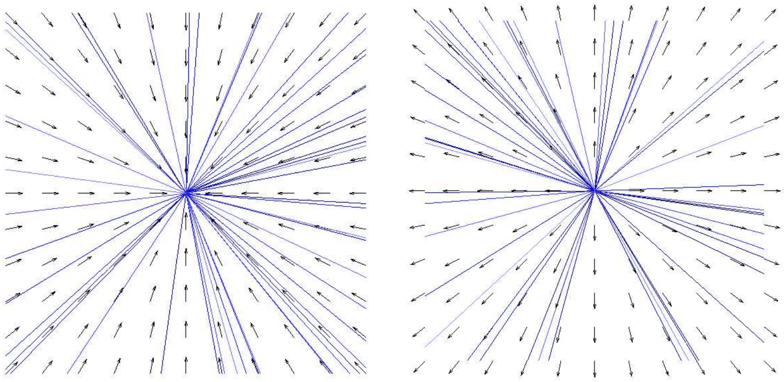

(a) attracting star (b) repelling star

Figure 3.1: Stars

Critical points are positions **p** in a vector field **V** where the vector vanishes, i.e. $\mathbf{V}(\mathbf{p}) = 0$. There are three main types of critical points: attractors, repellors and saddles. The streamlines around a repellor all seem to come out of it. An attractor has only streamlines directed into **p**. A saddle point has both, integral curves emanating from it and integral curves ending in it. Repellors are called sources and attractors are called sinks when talking about a flow field.

Looking at the form of the streamlines which end at a critical point yields three other types of description for critical points. If all integral curves ending at a point are straight lines, the point is called a star. As can be seen in figure 3.1, there exist repelling and attracting stars.

A critical point where not all, but some streamlines are straight lines is called node. Here, there are different velocities for the influx or outflux in different directions. This results in curved streamlines like in figure 3.2. Nodes can be repelling or attracting. If the mentioned velocities differ in sign, we have the special case called saddle. A saddle has repelling and attracting components.

Points where all streamlines are curved are called spirals. They can vary in the direction of the lines and in the direction of the velocity. This means, they may be repellors or attractors and the direction of rotation can be clockwise or counter-clockwise. In figure 3.3 both spirals have a clockwise rotation.

The special case of spirals are cycles. They are neither repellors nor attractors. While a saddle is repelling and attracting, a cycle does none of both. Cycles, as special case of spirals, may also rotate clockwise or counter-clockwise .

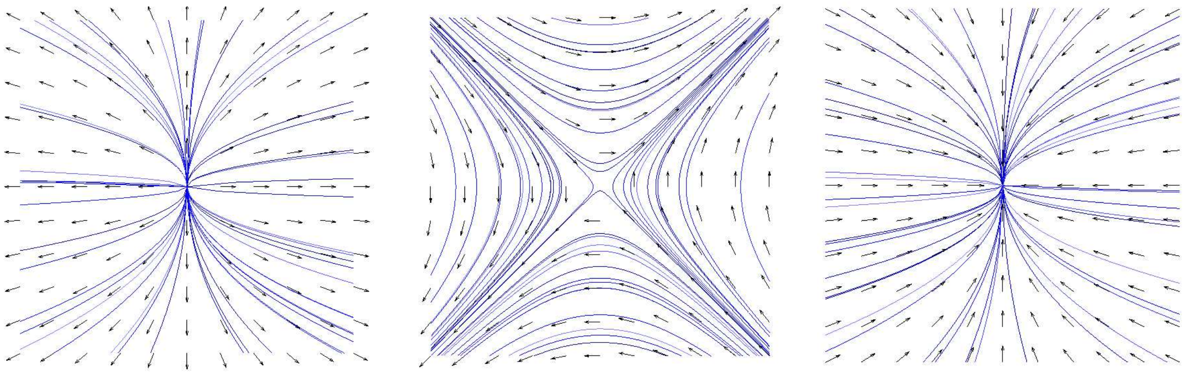

(a) repelling node (b) saddle (c) attracting node

Figure 3.2: Nodes and saddle

The critical points mentioned above appear in two dimensional vector fields. Some of them, like the stars, can be easily extended to their counterparts in three dimensions. But some critical points can only be expressed by combinations of the 2D cases.

Abraham [AS83] lists the commonly appearing 3D cases. They are composed of a plane with a repelling or attracting star or spiral and of a linear attractor or repellor in a direction not lying in the plane. This yields eight cases: 2 repellors with a repellor in the plane and a linear repellor, 2 attractors with an attractor in the plane and a linear attractor and 4 saddles with an attractor in the plane and a linear repellor, or vice versa.

A mathematical classification of all of the above named critical points can be found in an article of Nielson [NJ99].

Vortices

In the field of fluid flow vortices are very important. Unfortunately, like for features, there exists no general definition of what a vortex is. Everyone employed with vortices has an idea of what a vortex is, but scientist are not able to give more precise details than a few properties common to most vortices. So, vortices are sometimes viewed as an informal notion. Roth [Rot00] summarizes many attempts of defining vortices and describes the problems of the approaches.

To at least have a vague idea of what will be called vortex in the following of this thesis, we try a definition:

> A vortex is a flow pattern. This pattern has to have a certain size so that not every small eddy is treated as vortex. The size should be large enough, such that the pattern has a certain importance for the flow in the viewed region. If

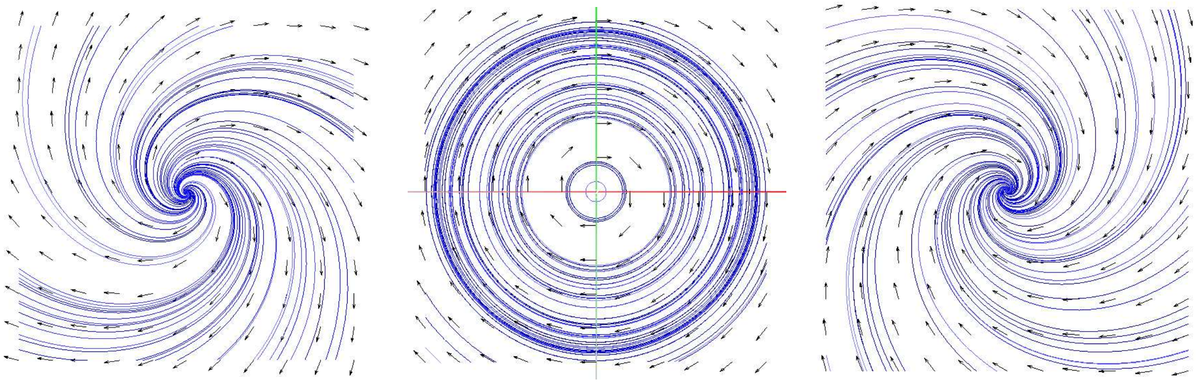

(a) repelling spiral (b) cycle (c) attracting spiral

Figure 3.3: Spirals and cycle

viewing from a particular direction onto a vortex, it looks like there is a circular or spiral-like flow.

This definition is not complete and may refer to itself in some way. It is just a sketch of what we call a vortex.

As known from the classification above (see subsection 3.1.1), the locations of vortices can be determined by lines (vortex cores) or by the region they cover. The research results for finding the core line of a vortex are much more advanced than for identifying the region it covers. The most important algorithms for finding vortex cores are explained and compared by Roth [Rot00].

3.2 Detection of vortex cores

Two vortex core detection methods shall be explained here to compare our results with the results obtained by these well-known algorithms. The first can be found in the comparison by Roth [Rot00]; it is the popular method by Sujudi and Haimes [SH95]. As second method we will describe very shortly the Clifford convolution approach by Ebling and Scheuermann [ES03].

3.2.1 Sujudi-Haimes

The basis for the eigenvector method proposed by Sujudi and Haimes is a tetrahedral grid. Every tetrahedron is handled separately. Since the vector field is linear in each tetrahedron, the corresponding, piecewise linear Jacobian $\mathcal{J}$ can be computed for each cell. As next and crucial step the eigenvalues of $\mathcal{J}$ are determined. If all eigenvalues are real, the tetrahedron is uninteresting and the algorithm steps to the next cell. The eigenvector for the remaining real eigenvalue has to be found as next step. Then, from the vectors located at the vertices of the tetrahedron their component in the eigenvector direction is subtracted. Again, now using the newly computed vectors, the Jacobian $\mathcal{J}_r$ has to be computed. With the already obtained quantities, a line with zero velocity, determined by the new vectors, can be computed. As last step, the intersection points of this line with the tetrahedron have to be determined. If there are two intersection points, their connection is a segment of the desired core line. Processing all tetrahedra and connecting the segments yields the vortex core lines of the vector field. Using this algorithm for comparison was very natural due to the fact that our datasets already had to be tetrahedral for the Helmholtz-Hodge decomposition.

3.2.2 Clifford convolution

The idea of transferring image processing methods to vector fields and thus getting new techniques for flow visualization was the origin for the approach presented by Ebling and Scheuermann. They use a product for vectors given in the Clifford algebra, define a convolution on vector fields and use it for pattern matching. Different masks for the convolution yield different resulting values. The values, also called similarities, measure how much the mask resembles the vector field at the position of application. The similarities are used to perform a pattern matching. It is important, that the pattern matching is orientation insensitive, i.e. it is not necessary that the pattern has a specific orientation in the field; patterns of any orientation can be found. Found patterns can be visualized by rendering isosurfaces of the similarities.

Detecting vortices is only a special case for the pattern matching. One just has to define masks representing a swirling flow and apply the convolution using these masks. Examples for results of this method can be found in the appendix A.2.

Chapter 4

Discrete Algorithms

4.1 Discrete Helmholtz-Hodge decomposition

The Helmholtz-Hodge decomposition is known from the smooth case (see section 2.5). Polthier and Preuß made a first attempt to define a discrete decomposition on irregular, triangulated grids [PP00, PP02]. This approach was extended to three dimensions by Tong et al [TLHD03].

The *FAnToM*-implementation of the three dimensional version used in this thesis is documented in Alexander Wiebel's project thesis [Wie03][1]. In the following it will be sketched how the 3D version works and some special properties will be mentioned.

4.1.1 Discrete 3D decomposition

Like in the two dimensional case, the algorithm applies to irregular grids. They must consist only of tetrahedra. For the discrete decomposition the input vector field has to be cell centered, i.e. inside each tetrahedron the vector field has to be constant. The potentials which appear during the decomposition are determined at the vertices of the grid and the field is interpolated piecewise linear between them. Having no cell centered field, it can be derived by taking the interpolated value at the barycenter for the whole cell.

To find the curl-free component of the field, a detour is taken. A search for a potential whose gradient is very similar to the original field is undertaken. Taking the gradient of this potential as first component, the desired vector field is obtained. It is similar to the input vector field and, as it is a potential field, it is guaranteed to be curl-free. For the divergence-free part an analog process yields the desired. The potential to search for, here is a vector potential instead of a scalar one. The curl of the vector potential is the desired

[1]The project thesis is only available in German and has not been published. The interested reader may contact project-thesis-2003@dergrosse.de to get a copy per email.

second component. Mathematically, the above means minimizing the following two integrals.

$$\begin{aligned} F(D) &= \frac{1}{2}\int_{\mathcal{V}} ||\nabla D - \mathbf{v}||^2 d\mathcal{V}, \\ G(\mathbf{R}) &= \frac{1}{2}\int_{\mathcal{V}} ||\nabla \times \mathbf{R} - \mathbf{v}||^2 d\mathcal{V}. \end{aligned}$$

Discretizing the conditions for the integrals to be minimal, yields two matrices. These matrices represent sparse linear systems and thus can be solved using iterartive techniques. The harmonic component can be obtained by subtracting the curl-free and the divergence-free component from the input vector field.

Uniqueness of the decomposition

Until now an important part of finding the potentials has been omitted. The minima of the integrals are not unique. To guarantee uniqueness of the decomposition extra conditions have to be introduced. Like in the smooth case, the uniqueness is achieved by requiring that $\mathbf{r}$ has to be tangential and $\mathbf{d}$ has to be orthogonal to the boundary. This is achieved by specifying the boundary values of the potentials. They are set to zero for the scalar potential and to the zero vector for the vector potential. This implies the desired properties for the components and thus their uniqueness. The boundary conditions are easily introduce into the linear system by setting the entries corresponding to boundary points to zero in advance.

Properties of the components

As mentioned in chapter 2, the components produced by the decomposition have very natural properties which enable the understanding of the structure of the vector field in a very intuitive way. While the rotation component has the same curl as the original field and thus contains all the vortices and eddies of the field, the field's sinks and sources appear in the divergence component. The harmonic component often is small or near constant for flows on simply connected regions.

The properties of the harmonic component led us to the assumption that it represents the part of a flow which only passes the regarded region. Searching for evidence for our assumption, we observed that when we added a Laplacian field to the original field it, up to numerical inaccuracies, reappeared in the harmonic component after the decomposition. An example for this can be viewed in the figures in appendix A.1. We studied examples with not-near-constant fields whose curl and divergence were zero and got results similar to the results for the above mentioned example. We will come back to our point in a later chapter trying to determine if this observation holds for all Laplacian fields.

4.2 Ridge and valley lines in 3D

The concept of ridge and valley lines for scalar fields is originated in the possibility to treat 2D scalar fields as height fields. Looking at a visualized height field, the similarity to a landscape or even mountain area is striking. Since in the real world the most interesting features of a landscape are its peaks, ridges and valleys, it is only natural to try to define these features for scalar fields too.

For easier understanding of 3D ridges and valleys we first have a look at how they are formally defined in two dimensions. Unfortunately there, again, exist several definitions. One, that can be easily extended for three dimensions and which almost implies a method to find the desired lines, is explained in the following.

Since a ridge is a line marking maximum height of a region in some way, it is natural that a ridge starts at a peak. The next point on the ridge is then the point which is the local maximum in the vicinity of the peak, ignoring the peak itself. Repeating this step, only accepting points which we not yet have found to lie on the ridge, we get a set of points. This set of points forms the ridge line. Thus, a ridge line can be seen as a line of minimal descent. The shortest definition of valley lines is that they are ridge lines of the negative height field. So beginning with a negative peak or minimum one can find criteria to define valleys that are analogous to the ones for ridge lines.

4.2.1 3D definition

Ridge and valley lines in a three dimensional scalar field have no obvious analog in nature, but they are known from fluid mechanics. A common definition for vortex cores are valley lines of pressure. A ridge in 3D has the main property that the values around it are smaller than the values at the position belonging to the ridge. Thus, we can use nearly the same criteria as for two dimensional data to define ridges. Starting at a local maximum of the scalar values, the next point belonging to a ridge is the maximum in the vicinity. The vicinity is a three dimensional region now, for example a sphere, and the starting point is again excluded when determining the maximum. The set of points resulting from repeatedly applying the definition forms the ridge line. Valley lines in 3D are defined analogously to the two dimensional case. We cannot speak of descent in 3D, hence we have to take the gradient in account. The following definition of Roth [Rot00] does exactly this:

> Ridge and valley lines are minimum lines of the [...] gradient.

The definition is cited here because it applies for both, the three dimensional and the two dimension case.

We found that Roth [Rot00] worked on valley lines in 3D and that he put down the above citation when we already had implemented our extraction algorithm. He mentions valley lines in connection with a method for finding vortex cores presented by Kida and Miura in [KM98], prior, and subsequent papers. They use 3D valley lines in a special pressure field to find vortex cores. In fact, we will also use ridge and valley lines to find vortex cores. As it will be explained later, we try to find valley lines in the norm of the vector potential produced by the 3D Helmholtz-Hodge decomposition.

4.2.2 Detecting ridges and valleys in 3D

Like mentioned before, our definition of ridge lines directly leads to a method for finding them. The definition above leaves an important point untouched: Most ridge lines do not end at a peak. There may be circumstances where this happens, but in general there are two or more lines emanating from the peak. In most cases there are two lines or in other words, one line running through the peak. To find the second line, one has to search for a maximum in the direction opposite to the first line. To exclude positions with large values, surrounding the first maximum, the search for the second has to be restricted to a certain angle around the opposite direction.

4.2.3 Implementation of the extraction algorithm in FAnToM

The ridge and valley lines extractor is implemented in *FAnToM*. It takes a three dimensional scalar field based on an arbitrary grid and displays the computed ridge and valley lines. The implementation of the 3D ridge lines extractor is an extension and improvement of an existing 2D algorithm originally developed by Xavier Tricoche, a former member of the visualization group of Dr. Scheuermann.

The algorithm is split into two parts. One part computes the points for the lines, a second part connects these points and displays the generated lines. Most of the work is done in the first part. However, the second part will be explained first, because it is much easier and shorter.

Displaying the lines

This step's input are two arrays with sets of points. Both arrays are structured similarly. The only difference is that one contains the points for the valley lines and the other for the ridge lines. Each of the arrays is processed in the same way. The valley lines are displayed in blue while the ridge lines' color is red.

All point sets contain vertices for the lines, each set for one line. The points represent the beginning of a line segment and the end of another. Lines are constructed using the `FgeLinesStrips` graphic primitive of *FAnToM*. All points belonging to a line, just have to be added using the `setNewVertex` function of the line-strips class.

Extracting the lines

As mentioned before, the main part of the extraction is performed in the first part of the algorithm. Central to this first step is a data structure that is used to record which positions are already processed and which are remaining. This data structure is named refarray in the implementation and so we will call it in the following. It is is implemented as a C++-struct. The struct's most important private attributes are two arrays. One of the arrays contains the indices of all currently processed positions, and the other is a list of booleans in which an element is set to true when the corresponding position is touched. To be able to access this structure easily the struct has the following public methods:

touch This method preforms the required updates of both arrays for a given index. A not yet mentioned attribute, containing the number of processed positions, is increased by one.

reset Each of the two arrays is reset to its initial state and the number of processed positions is set to zero by this method.

istouched For a given index, this procedure returns a boolean value depending on the state of the second array's element corresponding to the index.

setto All attributes of the refarray are set to the values of the input refarray's attributes, i.e. the input refarray is copied into the current.

update_and_reset This method does nearly the inverse of the previous. It marks all of the current refarray's processed positions as processed in the input refarray and resets itself.

Two major refarrays exist. One is for the maximum search and one for the line following. Some steps need their own, local refarray. The local refarrays are synchronized with the suitable major refarray after each step by using the `update_and_reset` method. The major advantage of using the refarray is a massive reduction of redundant processing.

In the following we will need the parameters controlling the extraction. A snapshot of the user dialog from the implementation can be found in the appendix C. The user has to specify the parameters there to adjust the behavior of the algorithm for his needs and his special dataset.

For the first step we need the "Extrema Neighborhood" (from now on EH) parameter. It determines the size of the neighborhood N in which we search. A value of one for EH means that while searching, we only take points into account which are directly adjacent to the currently processed position (from now on P). With a growing parameter value layers of positions, directly adjacent to the positions of the existing layers, are added to the searching area, A. These searching areas are called 1-neighborhood, 2-neighborhood and so on, depending on the layers of positions belonging to A. A 1-neighborhood is shown in figure 4.1(a). In figure 4.1(b) a two neighborhood is illustrated. The vertices with the red marker belong to the neighborhood of position P, which has the black marker.

Having explained this now, the first step is to find the maximum or minimum M in A. This is done by retrieving the values at the vertices belonging to the neighborhood and simply comparing them to the value at P. A position which appeared in any of the computed

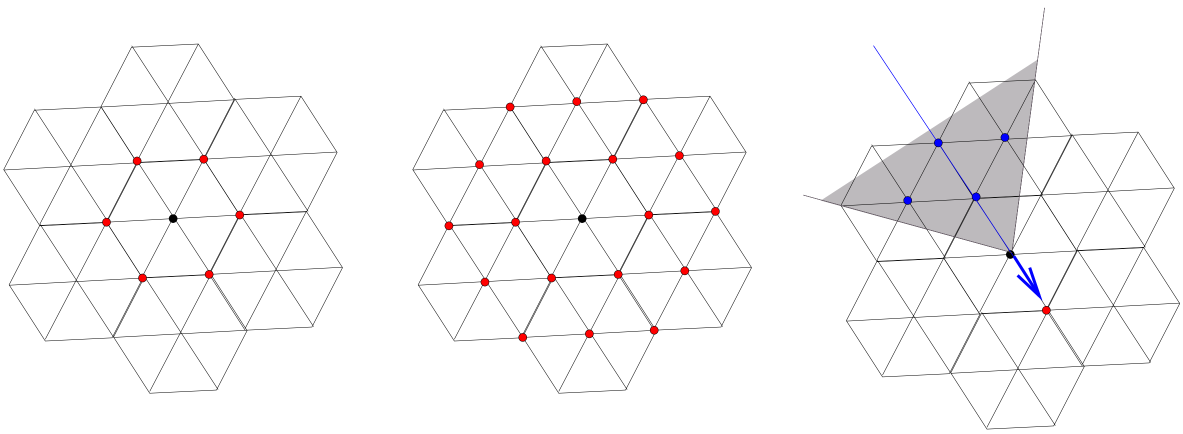

(a) one-neighborhood (b) two-neighborhood (c) Min cosine criterion

Figure 4.1: Neighborhoods

neighborhoods is marked as processed in the refarray. The maximum search is sequentially performed for all positions of the field not marked as processed yet. Positions found to be local extrema of A are stored in an array. Having processed all positions, we have two arrays. They hold all maxima respectively minima occurring in the field.

As already mentioned, most extrema lie in and not at the end of a ridge line. Hence, we have to look for two starting directions at every peak M. For the first direction, D, we search a new maximum[2] in the neighborhood of M. The vector $\mathbf{m}$ pointing from M to the maximum $\hat{M}$ represents the desired direction D. In figure 4.1(c) the maximum $\hat{M}$ is assumed to be at the red marked position. The vector $\mathbf{m}$ is represented by the blue arrow. A search for a maximum in the opposite direction $\hat{D}$ is performed to get the beginning of the second line. Both times the neighborhood to search is limited by the "Neighborhood Order"-parameter. The meaning of this parameter is similar to that of EH. In addition to this limitation, the second search accepts only points as maxima which lie in a zone determined by the "Min Cos" parameter. The parameter indirectly specifies an angle α by giving a lower bound for its cosine. As a large cosine means a small angle, the parameter specifies an upper bound for the angle. For the second direction $\hat{D}$ this means that a new point can only be accepted as maximum if the angle between the vector from M to this new point and the vector pointing in direction $\hat{D}$ is small enough. In the example in figure 4.1(c), the region where points may be accepted as maxima is highlighted by the grey area. Each

[2]In the following only the procedure for ridge lines is discussed because it is almost analog for valley lines.

of the two lines is followed directly after its direction is found. The following is performed for both directions identically.

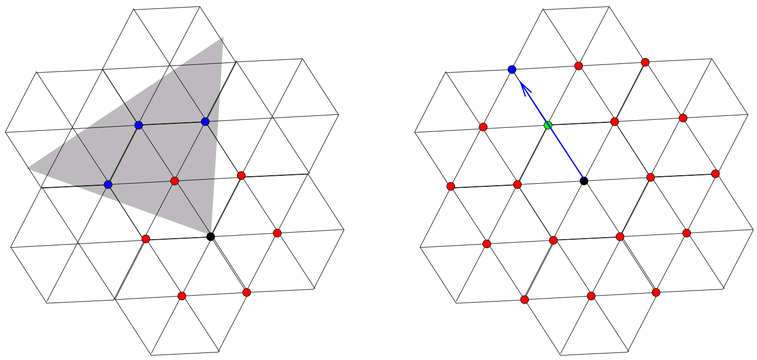

(a) Expanding the area. (b) Determining next point.

Figure 4.2: Steps of the following the lines.

Once a direction is determined the next point for the line is obtained by determining which of the one-ring neighbors lies in the direction differing least from D respectively $\hat{D}$. If a neighborhood order larger than one is considered, this point not necessarily has to be a maximum. In figure 4.2(b) the maximum is marked blue. This point has no connection to M. Thus, the green point will be the next point. In this example the green point lies exactly in the direction of the maximum, but in an example with a less regular triangulation or a larger neighborhood this is not necessary. The direction of the maximum is not recomputed for every new position. Most of the time the neighborhood is extended in the direction of the last computed direction. This is shown in figure 4.2(a), where the blue marked points are the extension. Points can belong to the extension only if their direction does not differ too much from the last computed direction. This, again, is limited by the "Min Cos"-parameter. How often the direction is newly computed is determined by the "Correction Frequency"-parameter, which represents the maximum of steps between two computations.

If a computation for the direction yields only points already processed, the line following ends. This can happen if the line runs into a corner of the dataset, if it crosses another line or if no maximum fullfilling the conditions set by the parameters can be found. When the following is aborted the "Min Length"-parameter comes into play. The number of segments belonging to a line is counted. Lines with less segments than "Min Length" are rejected and only the ones long enough are added to the array of lines. Filtering the lines in this way reduces the number of false positives and keeps only the lines with a certain importance to the field.

In the above steps, i.e. determining directions, following lines, extending neighborhoods and so on, visited positions are marked as processed in the refarray and hence omitted in the following steps. The figures only show 2D examples because it is easier to imagine how the examples would look in 3D than to construct understandable drawings for 3D examples.

Smoothing of the generated lines

A simple smoothing of the lines can be performed optionally. This takes place immediately before the lines are displayed. For every point $\mathbf{p}_i$, except the start and end-points, of a line the following equation is evaluated:

$$\hat{\mathbf{p}}_i := \mathbf{p}_i + \lambda(\mathbf{p}_{i-1} - 2\mathbf{p}_i + \mathbf{p}_{i+1}).$$

As the current point $\mathbf{p}_i$ shall be moved, an averaging with the two surrounding points is added to its position. $\mathbf{p}_{i-1}$ and $\mathbf{p}_{i+1}$ are the points surrounding, i.e. preceeding respectively following, the current point and the coefficient lambda specifies the strength of the smoothing. The lines are constructed using the corrected positions $\hat{\mathbf{p}}_i$ instead of the old $\mathbf{p}_i$ and then displayed.

Without the corrections, the line segments would just connect the points. Considering a grid with large cells and large angles of their edges this produces a very jagged curve. Using the correction yields a much smoother line which differs only in the jags while the general path is kept.

Chapter 5

Feature detection

5.1 Vortex detection by 3D ridge line extraction

As adumbrated in 4.2.1, the goal of defining a three dimensional version of ridges and valleys was to get a new method for vortex core detection. In the following the new method will be described and a theoretical explanation of why it works will be given.

5.1.1 The idea

The idea for the new method was initiated by a remark in the paper by Tong et al. [TLHD03], which presents the discrete 3D Helmholtz-Hodge decomposition. They say there that each vector in the vector potential represents a direction of rotation and an amplitude of the local vorticity. Then, they define vortices as local extrema of the norm of the vector potential. They propose to extract vortices by finding local extrema of the magnitude. From these points tube vortices can be tracked by following the piecewise linear curve of maximum vorticity. This line represents the vortex core.

The detection and tracking they mention work exactly like the extraction of the 3D ridge and valley lines as defined in this thesis before. Thus, the idea was to get the right scalar field, i.e. a field representing the magnitude of vorticity, and try to extract the ridges and valleys of this field. Due to the remark of Tong et al. the correct field for this purpose is the norm of the vector potential produced by the Helmholtz-Hodge decomposition, i.e. the potential that we call rotation potential.

5.1.2 The method

Due to the ideas mentioned above the Helmholtz-Hodge decomposition plays a central role for this method. It even provides the field to work on. Taking the field in which the vortices shall be detected, the first step is to perform the decomposition. Only the vector potential has to be extracted, the components and the scalar potential are not needed. The second step is to generate the desired scalar field. The field is derived by computing the norms, or magnitudes, of all vectors in the vector potential and treat them as the scalars at the position of the vector. Having obtained the scalar field the search for ridges and valley can be performed.

Care has to be taken when choosing the parameters for the ridge and valley line extractor. The “Extrema Neighborhood” and “Min Length” parameters determine the number of vortex cores detected. A large “Extrema Neighborhood” yields less maxima. If two vortices are located close to each other and the first parameter is chosen large, only the line for the stronger vortex is displayed. As the local maximum of the weaker vortex lies in the neighborhood of the stronger maximum, it is not treated as local maximum and the extraction of the associated line is omitted. A large value for the “Min Length” prevents short lines to be shown. Summarized, this means that weak and short vortices may be eliminated.

“Correction Frequency” and “Neighborhood Order” influence the form of the curves. Where the ridges and valleys get weaker, changing one or both of these parameters may yield an observable change of the lines extracted, for example vortex cores of weak vortices may end earlier then. The strong vortices can be found with most parameter values because they are explicit enough to leave the ridges and valleys extractor no choice.

The extracted lines at first do not look like vortex cores because they are very jagged. This can easily be overcome by the previously described smoothing.

5.1.3 Theoretical basis

Now the question arises, why the rotation potential has the properties referred to by Tong.

The answer can be found in an equation already mentioned in section 2.6:

$$\begin{aligned} \mathbf{R}(x) = & -\frac{1}{4\pi}\int_B \frac{1}{|x-x'|}\text{grad div } \mathbf{R}(x')dx' \\ & +\frac{1}{4\pi}\int_B \frac{1}{|x-x'|}\text{curl curl } \mathbf{R}(x')dx' \\ & -\frac{1}{4\pi}\int_{\partial B} \mathbf{R}(x')\frac{\partial}{\partial n(x')}\left(\frac{1}{|x-x'|}\right)dx' \\ & +\frac{1}{4\pi}\int_{\partial B} \frac{1}{|x-x'|}\frac{\partial \mathbf{R}(x')}{\partial n(x')}dx'. \end{aligned} \tag{5.1}$$

Discussion of the equation

To understand why equation 5.1 yields the desired properties for **R**, one has to look at its parts separately. The most interesting term is the second. The other terms will be treated as zero for the explanations in the following paragraph.

As known from 2.5, the curl of $\mathbf{R}$ is the rotation component $\mathbf{r}$ and the curl of $\mathbf{r}$ equals the curl of the original field. Hence $\nabla \times \nabla \times \mathbf{R}$ measures the vorticity of the examined vector field $\mathbf{v}$. Integrating the curl of $\mathbf{v}$ with the coefficient $\frac{1}{|x-x'|}$, is a distance weighted averaging of curl v in the neighborhood of the considered point x. This implies that at positions x where the curl of $\mathbf{v}$ is large in a vicinity the rotation potential has vectors with large magnitude. Additionally, the directions of the vectors of $\mathbf{R}$ are similar to those of the original field's curl.

For the above, the first, third and fourth term of 5.1 have been treated as being zero, but indeed they do not vanish. We will refer to them as error terms in the following. The first error term can be removed. This will be explained in subsection 5.1.4. The third and the fourth term of equation 5.1 are associated with the considered region's boundary ∂B. We were not able to eliminate these term, so their influence will be reported in subsection 5.1.5 .

5.1.4 Improvements

Since the first of the mentioned error terms comes from the divergence of the rotation potential, a divergence free rotation potential is desired. The Helmholtz-Hodge decomposition gives no hint as to whether the potential is divergence free or not. Experiments showed that in most datasets a non-negligible divergence is present. Remembering the properties of the fields produced by the Helmholtz-Hodge decomposition, one notices that the rotation component is divergence-free. As mentioned previously (see 4.1.1), the rotation component is the field most similar to the original field while being divergence free. Hence, the component seems to be the best choice as divergence-free alternative for the rotation potential $\mathbf{R}$. A problem is that the rotation component does not reflect the vector field at the boundary. Since the rotation component is always tangential to the boundary and the considered field has in general not this property, the rotation component can only help in the inner part of the field. As the method has problems at the boundary anyway, the rotation component has to be an improvement.

Our experiments showed a noticeable improvement. Examples and a detailed explanation of the improvements can be found in the chapter Results.

5.1.5 Drawbacks

As a drawback may be seen that the displayed lines do not give any hint to the strength or importance of a vortex core. In fact, this is a problem for our approach because the extraction of the ridge and valley line depends on the strength of the vortices. Especially in combination with special choices of the parameters for the extraction undesired results may be obtained. However, strong vortices are found nearly all the time.

Strong vortices may be missed if they are near the boundary of the grid. This leads to the second drawback, maybe the more important. Our algorithm has problems with any type of vortices, whether strong or weak, small or large, if they appear to be close to the boundary. The problem does not lie in the extraction algorithm, it lies in the potential used for the extraction. Having a look at equation 2.9 this is clear immediately. The two error terms which could not be eliminated both refer to the boundary. The factor $\frac{1}{|x-x'|}$ reduces the effect of the disturbing terms for points lying far away from the boundary. But for points near or on the boundary the denominator gets very small and thus the value of the whole fraction and with this the influence of the error terms increases fast.

5.2 Sinks and sources in 3D

In the previous section a description of a vortex core detection method is given. But vortex cores are not the only features in three dimensional flows. As mentioned in 3.1.2 there are other critical points of importance too. Sinks and source were named there. The Helmholtz-Hodge decomposition provides the potentials for a new approach to find such critical points. As suggested by Tong et al. [TLHD03], the potential for the curl-free component may be used for this task.

Since the potential is scalar, it is easy to find its maxima and minima. The rotation component is derived from the scalar potential by computing its gradient. Vectors in the component which are situated near positions of extrema of the potential, point directly onto, respectively away from, the positions. I.e. the flow diverges or converges in the vicinity of these positions. The maxima and minima themselves yield vanishing vectors and thus critical points. According to whether the flow in the vicinity diverges or converges these critical points are sinks or sources of the divergence component. As the divergence component contains all sinks and sources of the original field, the critical points are sinks and sources for the original field too.

The extrema can be found easily by comparing the neighbors of each vertex of the grid. The neighborhood can be chosen in different sizes (1-neighborhood, 2-neighborhood, and any larger neighborhood). A larger support for a neighborhood yields points which are maxima in larger areas. Thus, small sinks and sources which are nonrelevant can be pruned out. Small details may not only be not important, but can be noise introduced errors too. Using a larger neighborhood can filter out these errors.

5.3 Detecting Separation and attachment lines using 2D ridges and valleys

While examining which features possibly could be found using the Helmholtz-Hodge decomposition, we tried a new approach for finding separation and attachment lines. Separation and attachment lines are line type features which show where a flow separates or attaches, i.e. suddenly leaves respectively returns to a surface of a body.

Many approaches to detect separation and attachment have been proposed in literature. In a paper of Kenwright [Ken98] a good overview of the techniques presented before 1998 is given. First approaches simply placed many seed points along the considered surface and started stream or streak lines. If the number of positions is large enough the lines merge along the separation lines. Along attachment lines, the stream or streak lines diverge. It is also possible to compute skin friction lines. Skin friction lines are streamlines of the shear stress at the surface. These streamlines behave similar to the streamlines started near the surface. The problem with these and similar approaches (also discussed in the mentioned article) is that the observation and knowledge of the user is needed to find the region where the divergence or merge appears. Only newer techniques, like a topological approach and the algorithms published by Kenwright [Ken98, KHL99], can do the detection without the need of a user's knowledge, . For non-synthetical data with noise one could account an approach by Rao and Gillies [RG01], which extracts points of separation or attachment. An algorithm by Kenwright will be used for comparison with our technique in later examples. For a detailed description of the method the reader is referred to the previously mentioned papers by Kenwright.

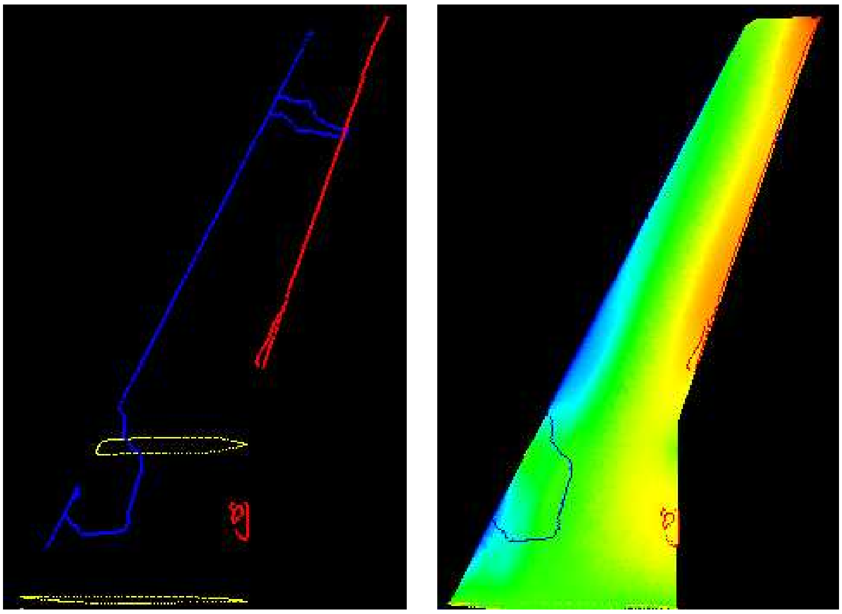

(a) (b)

Figure 5.1: (a) Ridge and valley lines of the divergence potential of the F6 wing, (b) the lines with the potential (upside of wing).

Our approach uses the potentials produced by the Helmholtz-Hodge decomposition. The origin for our computations is like for one of the above methods the shear stress at the body.

It is defined as the derivative of the velocity vector taken normal to the wall. As the field is defined on the surface of a body it can be processed by the two dimensional version of the decomposition. As the divergence potential is needed for our approach, the decomposition is performed only up to the step before computing the components from the potentials. Figure 5.1(b) shows the divergence potential of the shear stress at a wing of an F6 aircraft.

In agreement to the literature, we treat lines where the flow converges as separation lines and lines where it diverges as attachment lines. Having a potential for a field, it is easy to find positions of convergence and divergence. The most conspicuous positions are local extrema of the potential. As the the vector field is derived from the potential by computing the gradient, the vectors diverge or converge at the extrema. But there are more positions than solely the extrema. The flow diverges or converges also along ridge and valley lines in the potential. Hence these lines in the potential give the locations of the separation and attachment in the vector field.

5.3.1 Short summary of the technique

Summarized, what we do is the following: At first we compute the divergence potential of the flow, then we extract the ridges and valleys of the potential and treat these as lines of separation and attachment of the original field.

Our approach was tested mainly on two examples. The examples and the arising drawbacks of our approach will be presented in 6.3.1 and 6.3.2.

Chapter 6

Results

6.1 Problems of the 2D Helmholtz-Hodge decomposition

While experimenting with the 2D Helmholtz-Hodge decomposition, we found a remarkable drawback. The decomposition has problems handling features lying near or on the boundary.

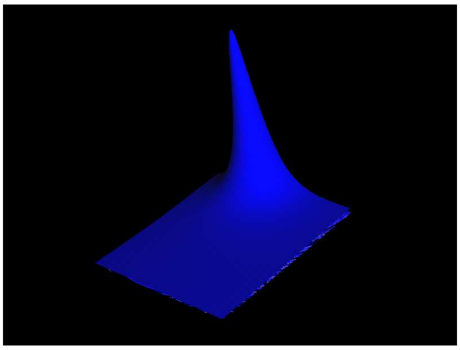

(a)

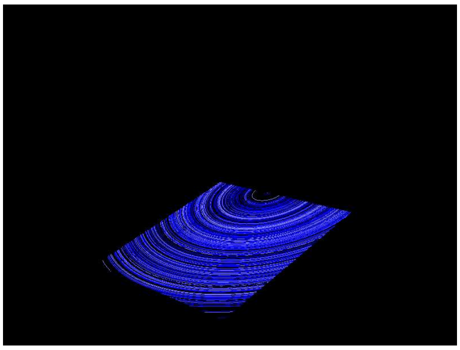

(b)

Figure 6.1: (a) Potential for original field, (b) streamlines in original field.

To examine the problems, we used an analytical example. Figure 6.1(a) shows a height field of the potential used to construct the vector field. Having only a single maximum and falling off equally in all directions, the potential is fairly simple. The maximum lies exactly on the boundary. Using this potential the vector field is constructed by computing the potential's gradient and rotating it 90 degrees in counter clockwise order. The derived vector field represents a cyclic flow (see 6.1(b)), its topology is as simple as its potential. The center of the rotation lies at the same position as the maximum of the potential.

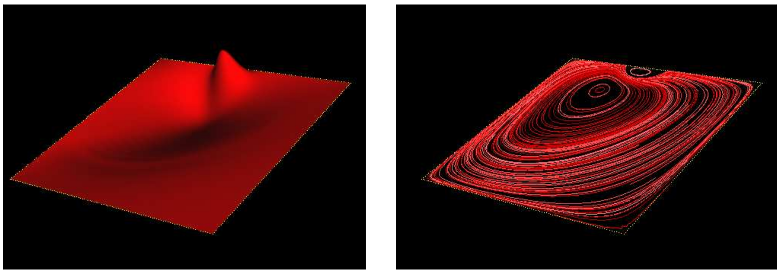

(a) (b)

Figure 6.2: (a) rotation potential, (b) rotation field

Experiments using potentials with maxima lying not to close to the boundary, yielded no problems. Indeed, the rotation potentials produced by the decomposition were nearly the same as the ones used to construct the fields. This was as expected, because a purely rotational field should be completely found in the rotation component.

However, decomposing fields with centers next to or on the boundary produces potentials that differ significantly from the original potentials. As can be seen in figure 6.2(a), the potentials magnitude is reduced very much. In the middle of the domain the sign of the potential is even inverted. This leads to a field which actually rotates in the reverse direction compared with the original field. Only a small rotation having the correct direction can be found near the maximum of the original potential. Both mentioned features can be recognized in figure 6.2(b) and in the zoomed section in figure 6.3(a).

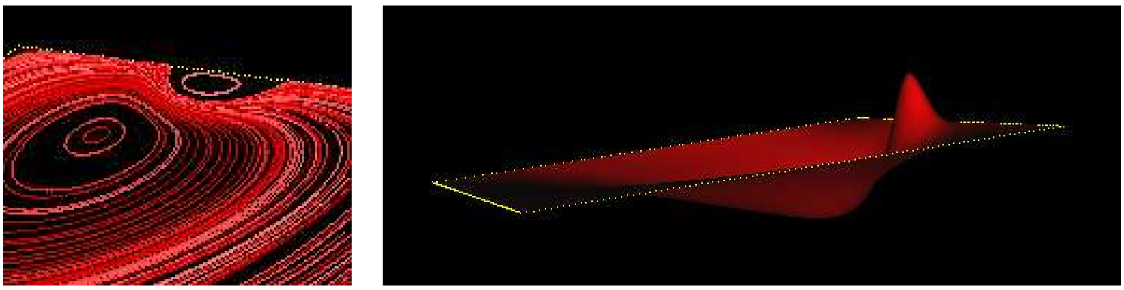

(a) (b)

Figure 6.3: (a) section of the rotation field, (b) the height field in 6.2(a) from another viewpoint

Tests with a potential having its maximum outside the boundaries of the field led to a rotation potential whose sign was inverted allover its domain. The rotation field showed a reverse directed circulation and a much smaller velocity compared to the original field. The center of this reverse rotation was completely different to that of the decomposed field. While the original center lay outside the boundaries, the new one was situated in the middle of the domain.

Summarized, the observed problems lead to significant changes in the structure of the fields. Indeed the topologies of the original fields have hardly anything in common with the topologies of their rotation components. We tried some workarounds to correct the deficiencies of the decomposition but achieved no reportable improvements. The only way to handle those problems seems to be, to work only with datasets were the interesting features are known to be not to close to the boundaries.

6.2 Vortex detection with 3D ridge lines

In the following, the results of applying the method presented in 5.1 to a test dataset will be described and discussed. At first the dataset itself will be described.

6.2.1 Examples

One of the datasets we used while working on the mentioned vortex extraction method was a simulation of the flow in a combustion chamber (GBK[1]). The chamber is used in central heating systems for normal houses. The data was generated by CFD simulation of the flow inside the chamber. The grid, shown in figure 6.4, illustrates the main geometry of the GBK dataset. It consists only of tetrahedra. Excluding the regions near the inlets, the vertices of the tetrahedra are distributed regularly and always eight of them form a cube. Each of these cubes is divided into the mentioned tetrahedra.

The dark grey lines in figure 6.4 represent the outer layer of the grid. Exhaust gas exits the chamber on the right plane of the grid in figure 6.4. The inlet for the gas is situated on the left in the figure. There, a higher density of lines can be recognized. Nine inlets for air can be found on the front and nine on the backside of the chamber. In figure 6.4 this again is indicated by lines lying closer together. As lines are the edges of the cells, at the inlets a higher resolutions of cells can be found. The higher resolution was chosen because the flow near the inlets is very turbulent. Although the whole flow in the chamber is very turbulent, the turbulence at the inlets is significantly higher. The eddying is no mistake of the design of the chamber, indeed it is desired to achieve a better intermixture of air and gas.

[1] from the German: **G**as**b**renn**k**ammer (brennen=to burn, kammer=chamber)

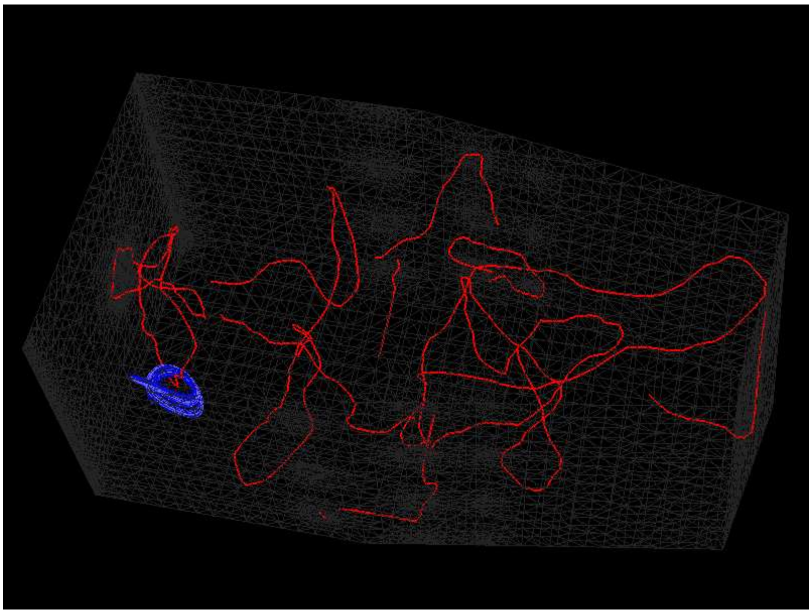

Figure 6.4: A vortex and extracted vortex cores in the combustion chamber.

6.2.2 Testing results

The methods of Sujudi and Haimes, and Ebling and Scheuermann will be compared with our method for vortex core detection (see section 5.1) in this subsection.

The first experiments were undertaken using the widely used method of Sujudi and Haimes. While their algorithm yielded very good results for many datasets tested before, the lines obtained for the GBK were rather confusing. Many short lines and false positives surrounded the important vortex cores. Due to the very turbulent flow this is not very surprising, but it reduces the usefulness of the method for analyzing the flow in the GBK very much.

Ebling and Scheuermann's approach provides a much clearer representation for the structure of the vortex cores. Some results of their pattern matching can be found in figure A.5. The similarities are represented by isosurfaces rendered using the marching tetrahedra algorithm. With the isosurfaces, vortex cores of not so distinct vortices can be suppressed or shown by rendering isosurfaces for higher respectively lower similarities.

Figure A.5 shows that results achieved with our technique, in the whole, agree with those obtained by the pattern matching. Disagreements appear close to the boundary. Especially the vortex located most right in the lower left image of figure A.5 is completely missed by our technique while the algorithm of Ebling and Scheuermann very explicity indicates that vortex. Examining the flow near the position of the vortex with streamlines supports this indication strongly. As the vortex is located near one of the outer edges of the dataset, it is close to two boundary planes. For our algorithm this is nearly the worst case. Only corners of the dataset, where there are three boundary planes are worse.

Results with improvement

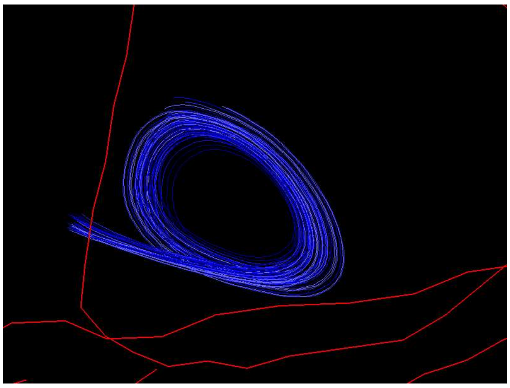

(a)

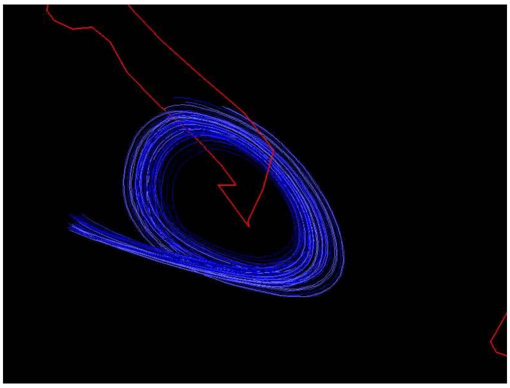

(b)

Figure 6.5: Cores extracted by the normal and the improved version

The improvement described in subsection 5.1.4 can help with two other problems. In figures 6.5 and 6.6 an example for the first case can be seen. Streamlines are drawn to give a hint where to expect the vortex cores. The figures show that the extracted lines moves closer to the line expected to be the vortex core when using the improved method. Two perspectives are given to provide an, at least vague, impression of the three dimensional constellation.

Improvements of this kind can be viewed if the extraction runs with the same parameters for both, the rotation potential and the rotation component of the rotation potential. Varying the parameters yields incomparable results. It is worth mentioning that not all lines are changed when using the improved method.

We noted above that the vortex near the edge of the dataset is missed by our algorithm. Another vortex possibly missed is the one near the gas inlet. Considering figure 6.8(a), one realizes that there are no lines close to the gas inlet, but looking at the streamlines in figure A.5 it is evident that there has to be core line. Additionally, the algorithm of Ebling and Scheuermann indicates a vortex there, in figure A.5 this is the second isosurface from the right. Even the method by Sujudi and Haimes extract a vortex core line there. Not detecting the core line for this vortex is the second problem with which the improved method helps.

In figure 6.7 isosurfaces for the divergence of the rotation potential are shown. Near the gas inlet a large divergence value can be noticed. As it will be shown, this large divergence is responsible for the algorithm to miss the colocated vortex.

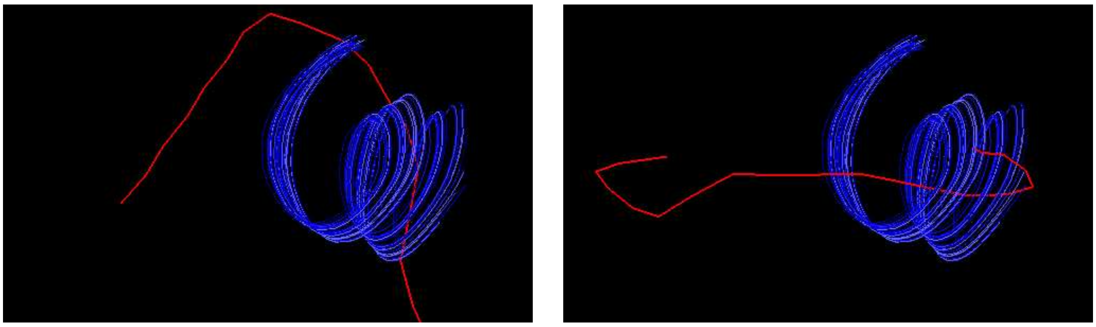

(a) (b)

Figure 6.6: Another perspective for the images in figure 6.5

Our improved algorithm uses the rotation component of the rotation potential. The divergence of this component, up to numerical inaccuracies, vanishes.

Extracting the ridge lines of the norm for the mentioned rotation component, yields lines near the gas inlet (see figure 6.8(b). This means, the vortex at the inlet is detected when using the potential without divergence. Thus, as stated above, the divergence near the inlet is the cause for missing the vortex there. Considering equation 5.1 this is not astonishing.

The presented examples show the advantage of using the divergence free rotation potential. Hence the extra work and time to get the rotation component of the potential is well spent.

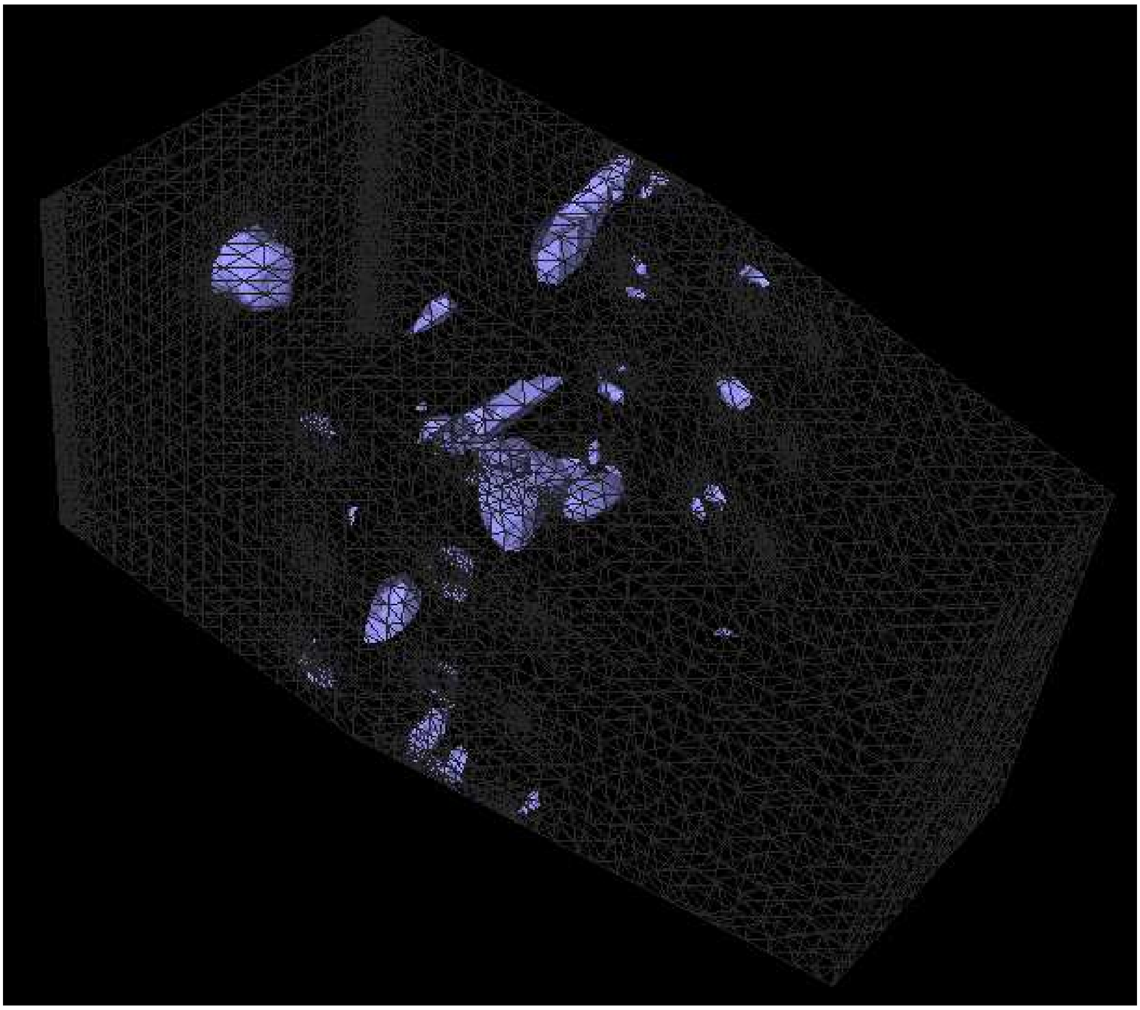

Figure 6.7: Isosurfaces for the divergence of GBK's rotation potential (value=15.0)

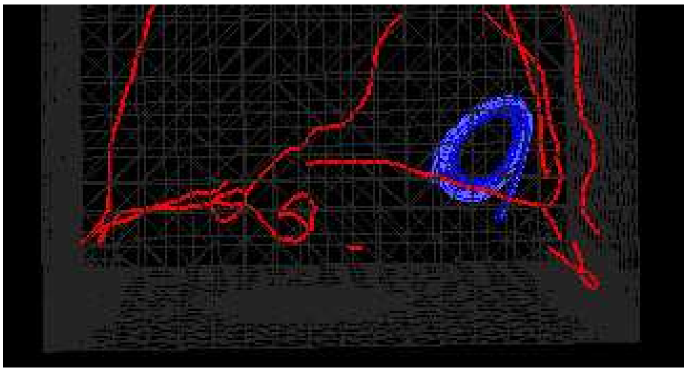

(a)

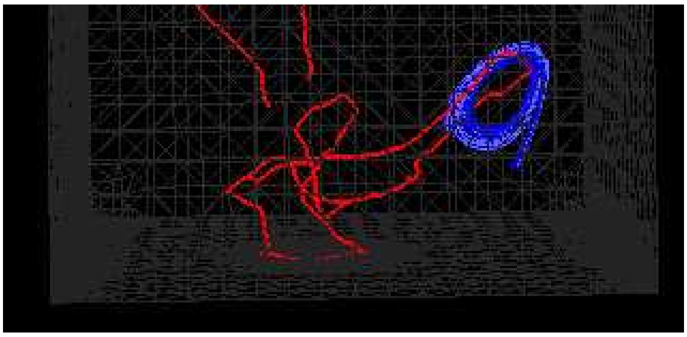

(b)

Figure 6.8: Improvement in an area with much divergence.

6.3 Extraction of separation and attachment lines

6.3.1 Examples

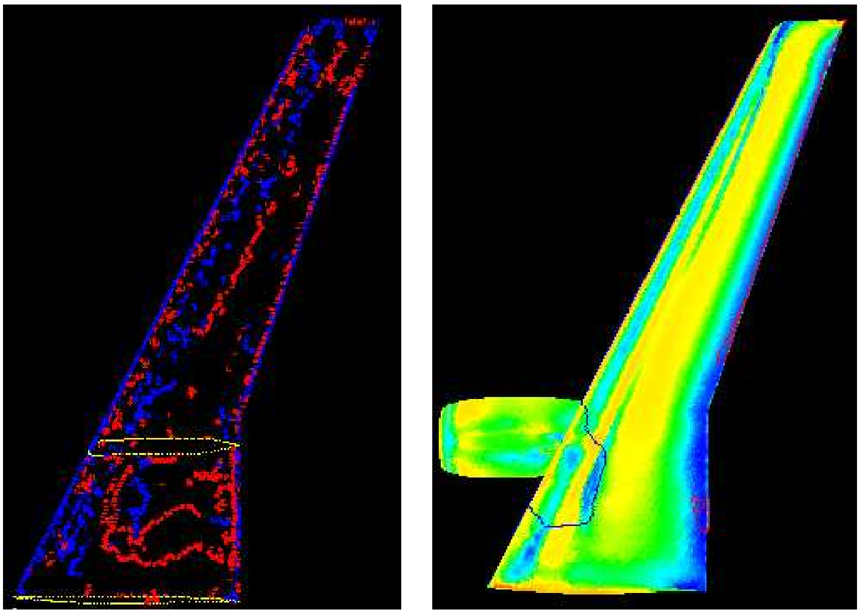

(a) (b)

Figure 6.9: (a) Separation and attachment computed with the algorithm of Kenwright, (b) velocity color map on wing and engine of F6 aircraft.

The first example for the separation-and-attachment-detection using ridge and valley lines, is a CFD simulation of the flow around a wing of an F6 aircraft. It has a shape typical for passenger airplanes. In figure 6.9(b) the wing and its engine are shown. A colormap for the velocity magnitude is applied. Figure 6.9(a) shows the results of the algorithm of Kenwright and yellow lines marking the boundaries of the grid. The boundaries arise through cutting the wing off the body of the aircraft and by the removal of the engine.

A delta wing dataset is the second example. Most of the present-day fighter aircrafts have geometries similar to the delta wing. While the wing's profile creates about 60% of the lift, the remaining 40% are induced by vortices caused by the delta-like geometry. The figures in appendix A.3 show the lines extracted by our method and LIC images. The LIC images give an impression of the flow on the surface.

In the first example the expected lines are found. An attachment process has to appear at the front of the wing and a separation at the back. Both main features are found by our algorithm, as shown by the lines in figure 5.1. There are only small disfigurements: The lines end in some distance to the grid boundaries while they are expected to continue. And the lines have turns near the boundary. But the results even look better than the ones obtained by Kenwright's algorithm.

For the second example our results are much worse than Kenwright's. Only short parts of the expected lines are extracted. A look at the divergence field shows that the separation and attachment lines of this component differ notably in shape, length and number to those of the original field, but that they are similar to the ridges and valleys extracted from the divergence potential. This yields that the problem is not originated in the ridges and valleys extraction but in the step before, i.e. in the decomposition.

The problems with the delta wing example and the disfigurements with the wing of the F6 will be discussed in the following.

6.3.2 Problems

Both mentioned problems appear close to the boundary. We know from previous sections that the 2D Helmholtz-Hodge decomposition does not work correctly near the boundary and that the vortex core extraction using ridge lines has trouble there too. We seem to have the same problem here.

As mentioned, the ridge and valley lines of the divergence potential of the delta wing are similar to the attachment and separation lines of the divergence component. But they are very different to the attachment and separation detected for the original field. So the processes of separation and attachment are not conserved well in the divergence component. A closer look leads to the insight that the lines look alike if the distance to the border is large enough. Thus the assumption from above, that the problems originate from the boundary, is correct.

While the separation and attachment lines in the delta wing dataset approach nearly tangential to boundary when coming closer to the front tip, the lines of the F6 wing are perpendicular to the boundary. As for the delta wing, the lines for the F6 dissappear near the border. Fortunately the lines for the wing are thus only truncated a little bit and the main structure is preserved.

The turns of the lines near the engine are also originate in the boundary problem. They can be avoided by changing some parameters of the ridges and valleys extractor; this results in slightly shorter lines and loss of very short lines. Thus, one has to decide here whether to get false turns or to lose some, possibly desired, features.

6.3.3 3D extraction of separation and attachment

We tried to experiment with a technique to find separation and attachment by inspecting the flow above the surface. Especially, we attempted to use the divergence component of the 3D vector field. We tried to find features in it that would give us hints for the locations of separation and attachment.

Unfortunately, we were not able to get reportable results because of two difficulties. The first was that we were not able to decompose some of the available 3D vector fields due to their size. Computing the components of one of these fields while holding the field itself in the memory was impossible because this exceeded the RAM of the used computer (3GB) by far. As this first difficulty occurred we tried smaller fields. The problem here, the second difficulty, was that none of the available data had attachment or separation strong enough to be easily detected.

Thus we have to wait for more powerful computers in our group to continue our experiments.

Chapter 7

Conclusion

In this thesis two new approaches for feature detection in flow fields have been presented. A method for vortex core extraction in three dimensional vector fields and an approach for separation and attachment line detection have been described. Both techniques base on two main algorithms: the Helmholtz-Hodge decomposition, in 2D and 3D, and a ridge and valley lines extraction, also for two and three dimensional fields.

The methods have been compared with known algorithms having similar goals to show their features, advantages and drawbacks. Furthermore, problems and drawbacks of the discrete Helmholtz-Hodge decompositions in two and three dimensions have been discovered. The causes for the problems have been described in the thesis. It is worth noting that the problems have not been mentioned in any of the three papers the methods were proposed in.

7.1 Future work

In various parts of this thesis diverse limits reached by the particular methods have been mentioned. Some limits appeared due to mathematical properties and thus can not be crossed. Other limits appeared because of the datasets and hardware available for the work.

The limits set by hardware and data leave subjects for future research. Finding datasets small enough for the decomposition and containing distinct separation and attachment processes, would pave the way for experiments on detecting these processes using the 3D flow features. Hardware with more main memory could also open this field of activity.

Availability of vector field data containing sinks and sources of interest would offer the possibility of developing algorithms for sink and source detection algorithms using the divergence component. Further experiments with the vortex detection can be undertaken when having datasets with vortices located far enough from the boundary.

It is yet unknown how the Laplacian parts of the vector fields are distributed over the components of the decomposition, but I am already working on a theoretical model for this.

Appendix A

Images

A.1 Hodge Decomposition

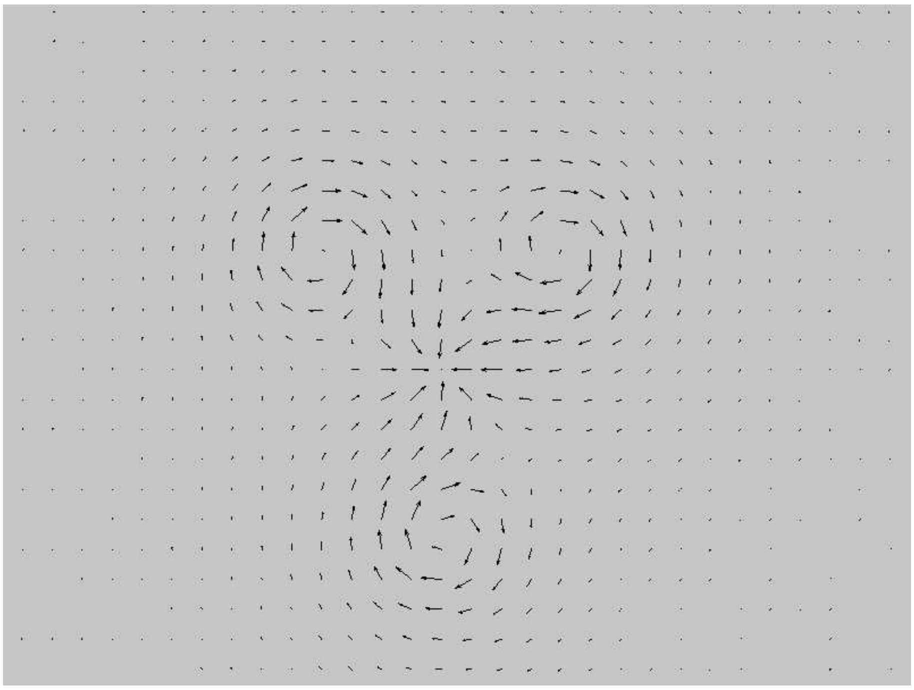

Figure A.1: A vector field containing three vortices and a sink

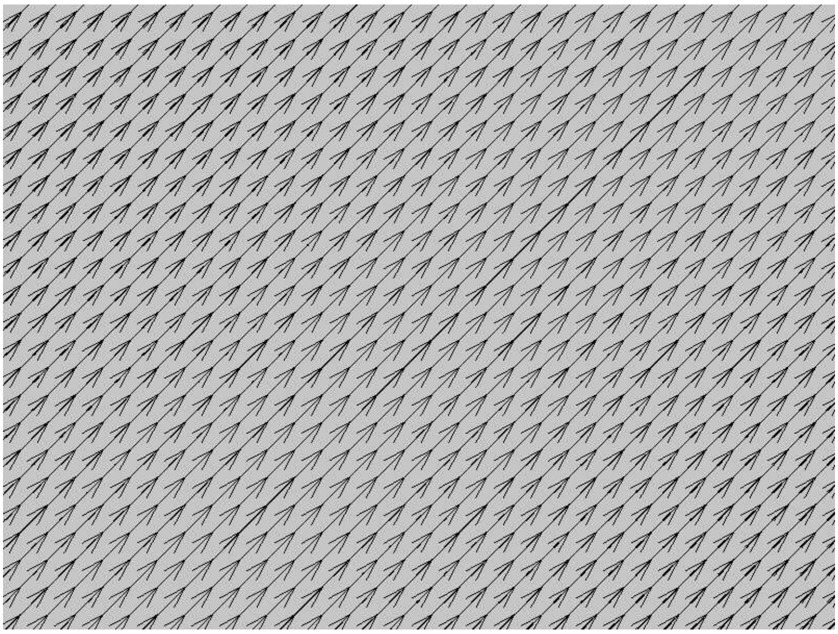

Figure A.2: A constant vector field. The norm of the vectors of this field is about ten times larger than in A.1

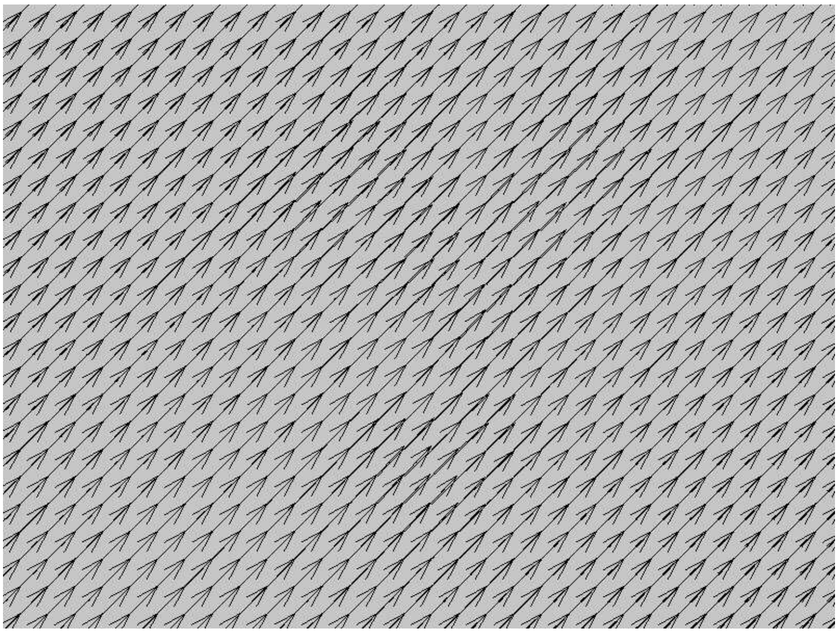

Figure A.3: Sum of A.1 and A.2. Only the influence of the large constant vector field is visible.

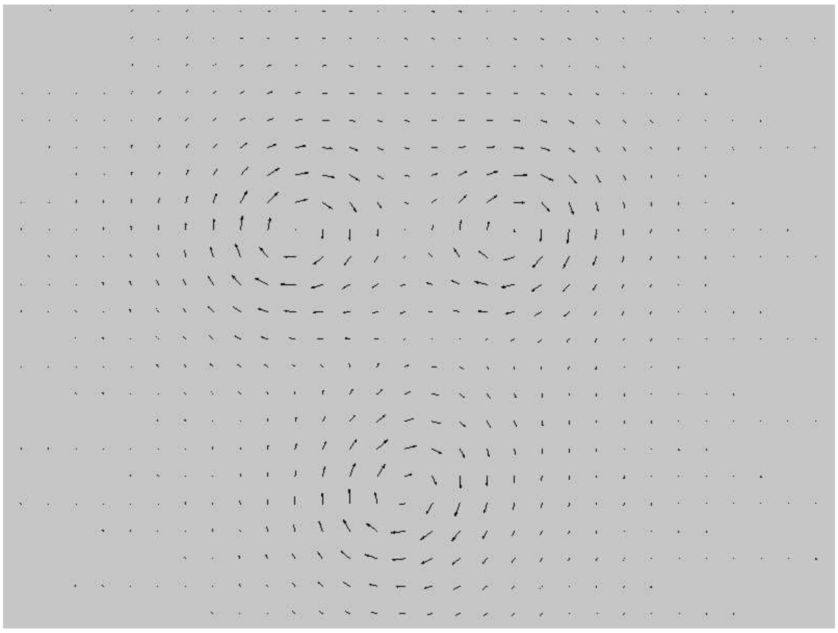

Figure A.4: The extracted divergence-free component of the field in A.3.

A.2 Vortex core lines

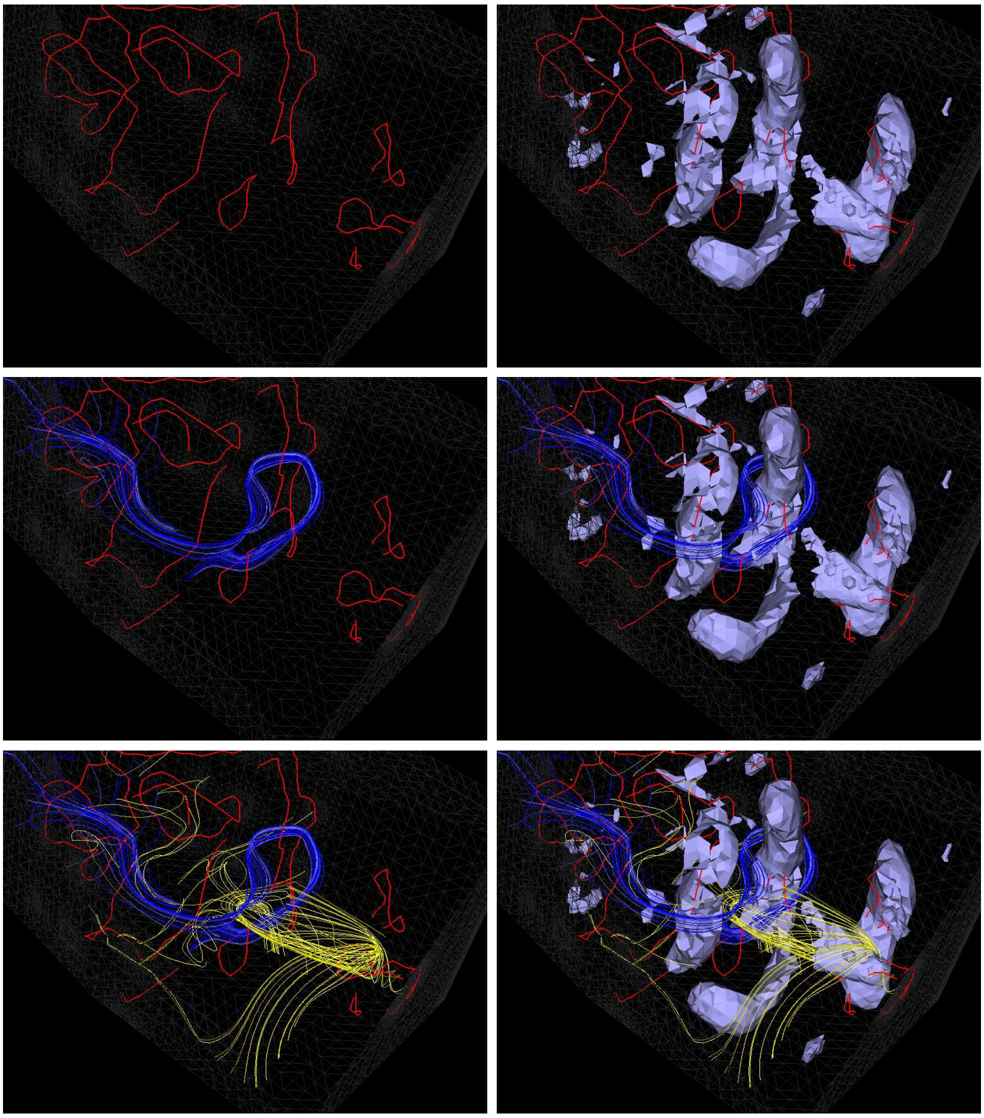

Figure A.5: Vortex core lines extracted by ridge lines, isosurfaces of the similarities computed by the Clifford convolution and streamlines of the flow in the combustion chamber.

A.3 Separation and attachment lines

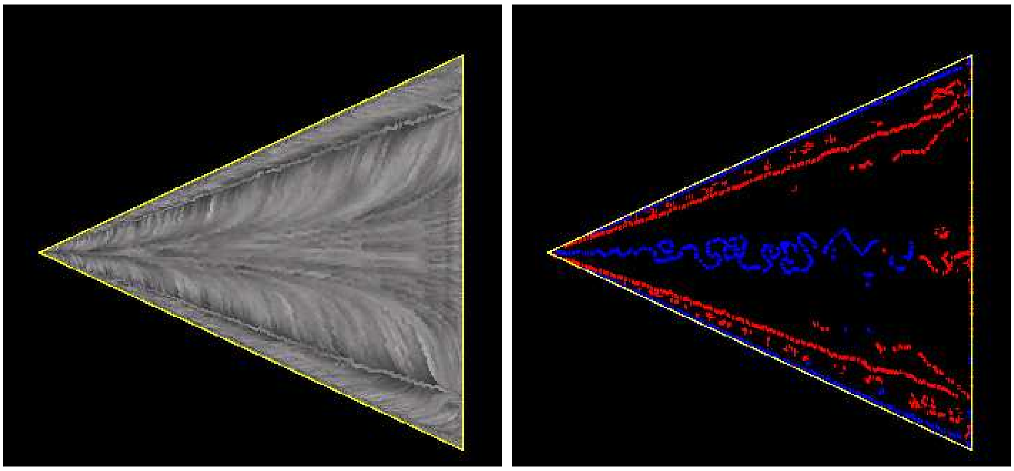

Figure A.6: LIC image, and separation and attachment lines of shear stress field of delta wing dataset.

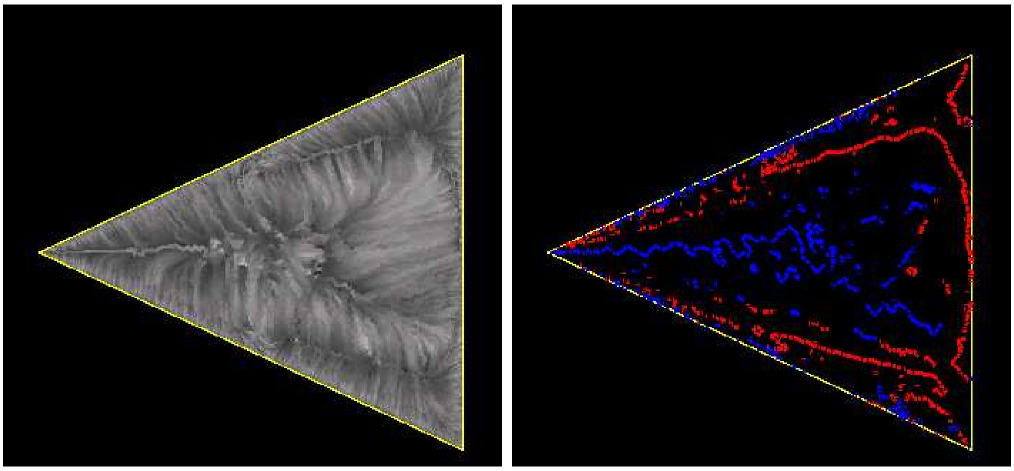

Figure A.7: LIC image and separation and attachment lines of the divergence component of the field in figure A.6.

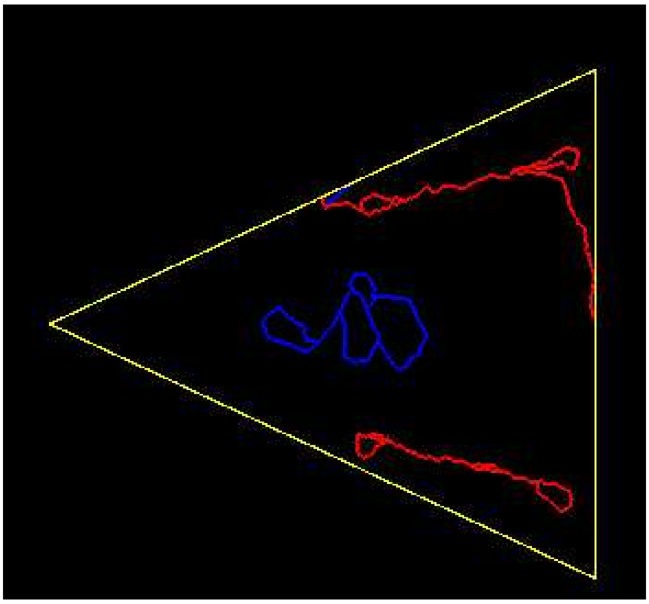

(a)

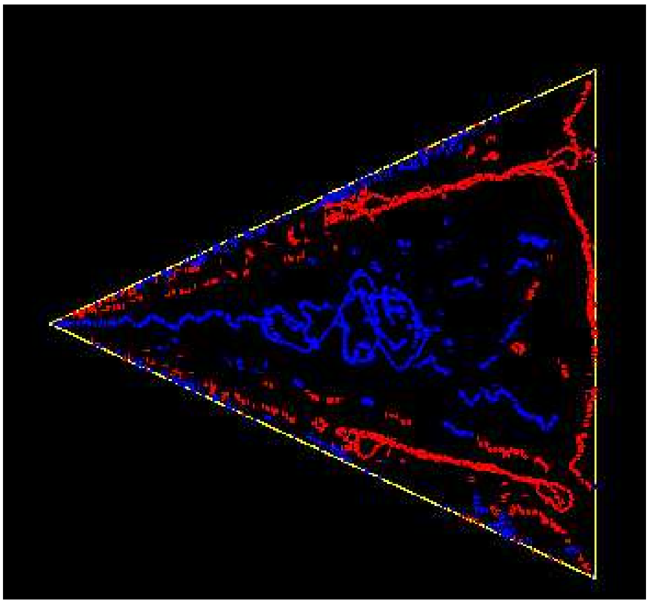

(b)

Figure A.8: (a) Ridge and valley lines of the divergence potential of the field in figure A.6, (b) The ridges and valleys like in (a) with the separation and attachment lines from figure A.7

Appendix B

Formulary

In this part of the appendix some identities from vector analysis and other in the thesis used mathematical facts are noted.

B.1 Some Properties of differential operators

At first the already mentioned but basic identities:

$$\begin{aligned} \nabla U &= \text{grad } U & \text{(B.1)} \\ \nabla \cdot \mathbf{V} &= \text{div } \mathbf{V} & \text{(B.2)} \\ \nabla \times \mathbf{V} &= \text{curl } \mathbf{V} & \text{(B.3)} \\ \Delta U &= \nabla \cdot \nabla U = \text{div grad } U. & \text{(B.4)} \end{aligned}$$

Now some equations in which ∇ is applied twice:

$$\begin{aligned} \nabla \times \nabla U &= \text{curl grad } U = 0 & \text{(B.5)} \\ \nabla \cdot (\nabla \times \mathbf{V}) &= \text{div curl } \mathbf{V} = \mathbf{0} & \text{(B.6)} \\ \Delta \mathbf{V} &= \text{grad div } \mathbf{V} - \text{curl curl } \mathbf{V}. & \text{(B.7)} \end{aligned}$$

For all operators $o \in \{\text{grad}, \text{curl}, \text{div}, \Delta\}$ it holds that

$$\begin{aligned} o(X+Y) &= o(X) + o(Y) & \text{(B.8)} \\ o(cX) &= c\, o(X), & \text{(B.9)} \end{aligned}$$

where the fields X, Y and the constant c are scalar or vector valued depending on the operator.

As mentioned in chapter 2, the notation using the nabla operator can be a little bit confusing in some cases. Thus, it should be said here again that the following three are completely different:

$$\nabla^2 \equiv \nabla \cdot \nabla \equiv \Delta \equiv \text{div grad} \tag{B.10}$$

$$\nabla(\nabla) \equiv \text{hessian} \equiv \text{grad grad} \tag{B.11}$$

$$\nabla(\nabla \cdot) \equiv \text{grad div} . \tag{B.12}$$

B.2 Characteristics of harmonic functions

In the following, let $\varphi : \mathbb{R}^n \to \mathbb{R}$ be a harmonic function, i.e. $\Delta\varphi = 0$. The following holds for harmonic functions.

- Let φ be non-constant in a region B, then it has no extrema in B.
- Let $c \in \mathbb{R}$ be a real valued constant.

$$\varphi|_{\partial B} = c \quad \Rightarrow \quad \varphi(\mathbf{r}) = c, \forall \mathbf{r} \in B$$

- Let $\varphi, \hat{\varphi}$ be two harmonic functions.

$$\varphi|_{\partial B} = \hat{\varphi}|_{\partial B} \quad \Rightarrow \quad \varphi = \hat{\varphi}$$

Appendix C

FAnToM-GUI

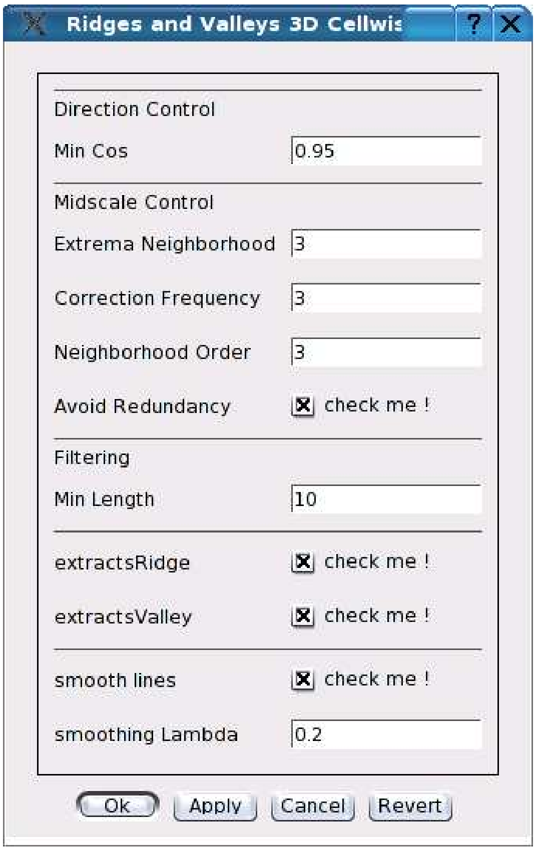

Figure C.1: Dialog for ridge and valley lines extraction algorithm.

Bibliography

[AMR88] R. Abraham, J. E. Marsden, and T. Ratiu, editors. *Manifolds, Tensor Analysis and Applications*, volume 75 of *Applied Mathematical Science*. Springer, 1988.

[AS83] Ralph H. Abraham and Christopher D. Shaw. *Dynamics: The Geometry of Behaviour*, volume 2. Aeriel Press, 1983.

[BSMM00] Ilj́a N. Bronstein, Konstantin A. Semendjajev, Gerhard Musiol, and Heiner Mühlig. *Taschenbuch der Mathematik*. Verlag Harri Deutsch, Thun und Frankfurt am Main, fünfte edition, 2000.

[BSTW02] Holger Burbach, Gerik Scheuermann, Xavier Tricoche, and Thomas Wischgoll. *FAnToM(Field Analysis by Topological Methods)*. AG Graphische Datenverarbeitung und Computergeometrie, University of Kaiserslautern, 1.1 edition, 2002.

[BT79] A. I. Borisenko and I. E. Tarapov. *Vector and Tensor Analysis with Applications*. Dover Publications Inc., New York, 1979.

[CM98] Alexandre J. Chorin and Jerrold E. Marsden. *A Mathematical Introduction to Fluid Mechanics*, volume 4 of *Texts in Applied Mathematics*. Springer-Verlag, New York, third edition, 1998.

[ES03] Julia Ebling and Gerik Scheuermann. Clifford convolution and pattern matching on vector fields. In *Proceedings of IEEE Visualization '03*, Los Alamitos, CA, 2003. IEEE Computer Society.

[HH89] James Helman and Lambertus Hesselink. Representation and display of vector field topology in fluid flow data sets. *Computer*, August 1989.

[Ken98] David N. Kenwright. Automatic detection of open and closed separation and attachment lines. In *Proceedings of IEEE Visualization '97*, pages 151–158, 1998.

[KHL99] David N. Kenwright, Chris Henze, and Creon Levit. Feature extraction of separation and attachment lines. *IEEE Transactions on Visualization and Computer Graphics*, 5(2):135–144, April-June 1999.

[KM98] Shigeo Kida and Hideaki Miura. Identification and analysis of vortical structures. *European Journal of Mechanics - B/Fluids*, 17(4):471–488, 1998.

[MDB87] Bruce H. McCormick, Thomas A. DeFanti, and Maxine D. Brown, editors. *Visualization in Scientific Computing.* ACM SIGGRAPH, New York, 1987.

[NJ99] Gregory M. Nielson and Il-Hong Jung. Tools for computing tangent curves for linearly varying vector fields over tetrahedral domains. *IEEE Transactions on Visualization and Computer Graphics*, 5(4):360–372, October-December 1999.

[PP00] Konrad Polthier and Eike Preuss. Variational approach to vector field decomposition. In R. van Liere, F. Post, and et. al., editors, *Proc. of Eurographics Workshop on Scientific Visualization.* Springer Verlag, 2000.

[PP02] Konrad Polthier and Eike Preuss. Identifying vector field singularities using a discrete hodge decomposition. In H. C. Hege and Konrad Polthier, editors, *Visualization and Mathematics III.* Springer Verlag, 2002.

[RG01] Anil Rao and Duncan Gillies. Separation and attachment point feature extraction from 2d cardiac MR blood flow images. In *Medical Image Understanding and Analysis - Conference Proceedings*, 2001.

[Rot00] Martin Roth. *Automatic Extraction of Vortex Core Lines and Other Line-Type Features for Scientific Visualization.* PhD thesis, ETH Zürich, 2000.

[SH95] David Sujudi and Robert Haimes. Identification of swirling flow in 3-d vector fields. In *12th AIAA CFD Conference*, San Diego CA, June 1995.

[TLHD03] Yiying Tong, Santiago Lombeyda, Anil N. Hirani, and Mathieu Desbrun. Discrete multiscale vector field decomposition. In *SIGGRAPH 2003 Proceedings.* ACM, 2003.
`http://www-grail.usc.edu/pubs/TLHD03.pdf`.

[Wie03] Alexander Wiebel. Tetrahedrisierung irregulärer Gitter und 3D-Helmholtz-Hodge-Zerlegung von Vektorfeldern. Projektarbeit, University of Kaiserslautern, Fachbereich Informatik, AG Visualisierung, July 2003.